

This is an Open Access document downloaded from ORCA, Cardiff University's institutional repository: <https://orca.cardiff.ac.uk/id/eprint/155453/>

This is the author's version of a work that was submitted to / accepted for publication.

Citation for final published version:

Maier, Wolfgang , Barnes, Stephen J., Godel, Belinda M., Grobler, Danie and Smith, William D. 2023. Petrogenesis of thick, high-grade PGE mineralisation in the Flatreef, northern Bushveld Complex. *Mineralium Deposita* 58 , pp. 881-902. 10.1007/s00126-022-01156-6

Publishers page: <https://doi.org/10.1007/s00126-022-01156-6>

Please note:

Changes made as a result of publishing processes such as copy-editing, formatting and page numbers may not be reflected in this version. For the definitive version of this publication, please refer to the published source. You are advised to consult the publisher's version if you wish to cite this paper.

This version is being made available in accordance with publisher policies. See <http://orca.cf.ac.uk/policies.html> for usage policies. Copyright and moral rights for publications made available in ORCA are retained by the copyright holders.





Petrogenesis of thick, high-grade PGE mineralisation in the Flatreef, northern Bushveld Complex

Wolfgang D. Maier¹ · Stephen J. Barnes² · Belinda M. Godel² · Danie Grobler³ · William D. Smith^{1,4}

Received: 15 October 2021 / Accepted: 2 December 2022
© The Author(s) 2023

Abstract

The Flatreef of the northern limb of the Bushveld Complex is a world-class platinum-group element (PGE) deposit representing the down-dip extension of the Platreef. Exploration drilling in the central portion of the project area intersected a particularly thick PGE-mineralised portion of the Flatreef exposed in drill core TMT006 and its two deflections, containing 4.5 ppm PGE (Pt + Pd + Rh + Au) over 90 m and ~3.7 ppm PGE over 150 m. Data obtained using whole rock geochemical analysis, field emission scanning electron microscopy, micro X-ray fluorescence and X-ray computed tomography indicate that the PGE are hosted by, or are spatially closely associated with, disseminated sulfides that occur interstitial to the cumulus silicate minerals. PGE grades show a broad, albeit irregular trend of progressive downward decrease, whereas most metal ratios (Cu/Ni, Pt/Rh, Cu/Pd and, to a lesser degree, Pt/Pd) remain broadly constant throughout the 90 m main ore zone. These features are interpreted to reflect two stages of ore formation: (i) hydrodynamic concentration of sulfidic ultramafic crystal mushes and (ii) localised downward percolation of sulfide melt in response to fluidisation of the cumulate mush caused by infiltration of ascending magmatic or crustal fluids. The model is consistent with the close spatial association of the sulfides with interstitial plagioclase as well as accessory phlogopite, quartz, apatite and rutile, whereas cumulus orthopyroxene is largely free of sulfide.

Keywords Platinum-group elements · Bushveld Complex · Flatreef · Platreef · South Africa

Introduction

Prospection of the Platreef of the Bushveld Complex, South Africa, on the farms Turfspruit and Macalacaskop started in 1998, focussing initially on the delineation of mineralization that could support open-pit mining (Grobler et al. 2019). Deep drilling commenced in 2007 and established that at a depth of approximately 600 m the dip of layering of the Platreef intermittently flattens for a distance of about 1–2 km in the dip-direction, from ~40° to sub-horizontal. At

the same time, the mineralised layers thicken, to commonly several 10 s of metres (Grobler et al. 2019). This led to the coining of the term “Flatreef” (Kekana 2014). The most recently declared mineral resource for the Flatreef is 42 Moz PGE (346 Mt @ 3.8 g/t Pt + Pd + Rh + Au, 0.32% Ni and 0.16% Cu) (<https://www.ivanhoemines.com>), making it one of the largest PGE deposits on earth. The TMT006 drill core intersections, including the mother hole and two deflections (hereafter abbreviated D₀, D₁ and D₂, respectively), expose a particularly thick portion of the Flatreef containing 4.5 ppm Pt + Pd + Rh + Au over a thickness of 90 m and a further ~2 ppm over the underlying 60-m interval. Understanding the origin of the variation in grade across the Flatreef is of relevance for mining and exploration, but interpretations are hampered by widely spaced drill cores. In the absence of outcrop and underground exposures, the TMT006 drill cores offer a unique opportunity to study lateral variation in layering and grade on a relatively small scale, i.e. over a few metres at the most. Also, the TMT006 drill cores represent the richest of the more than 600 intersections drilled on the Turfspruit property,

Editorial handling: M. Fiorentini

✉ Wolfgang D. Maier
maierw@cardiff.ac.uk

¹ School of Earth and Environmental Sciences, Cardiff University, Cardiff, UK

² CSIRO, 26 Dick Perry Ave, Kensington, WA 6151, Australia

³ Ivanplats Ltd, Mokopane, South Africa

⁴ Present Address: Department of Earth Sciences, Carleton University, Ottawa, Canada

rendering their study particularly interesting. In the present paper, we focus on characterising and interpreting the PGE geochemistry of the drill core intersections, complementing the work of Stephenson (2018) on a suite of samples from D₂ which focussed on mineral chemical data and S isotopes in addition to whole rock data.

Geology and stratigraphy

The Turfspruit project area is located ~15 km to the N of Mokopane, in the northern limb of the Bushveld Complex (Fig. 1A, B). Grobler et al. (2019) established that the

Flatreef is the downdip extension of the Platreef Unit, both being correlatives of the Upper Critical Zone (UCZ) in the eastern and western Bushveld Complex, including the UG2, Merensky and Bastard reefs (Fig. 1C). The TMT006 drill cores intersect the flattened central domain of the Flatreef project area (ESM 1-S1, Maier et al. 2021a), namely the interval from the lower Main Zone across the Bastard and Merensky cyclic units and into the strongly contaminated footwall of the Merensky Reef. These footwall rocks are characterised by abundant metasedimentary xenoliths and were thus grouped into the “Footwall Assimilation Zone” (FAZ) by Grobler et al. (2019). The detailed stratigraphy of the Flatreef is shown in Fig. 1C and comprises the following

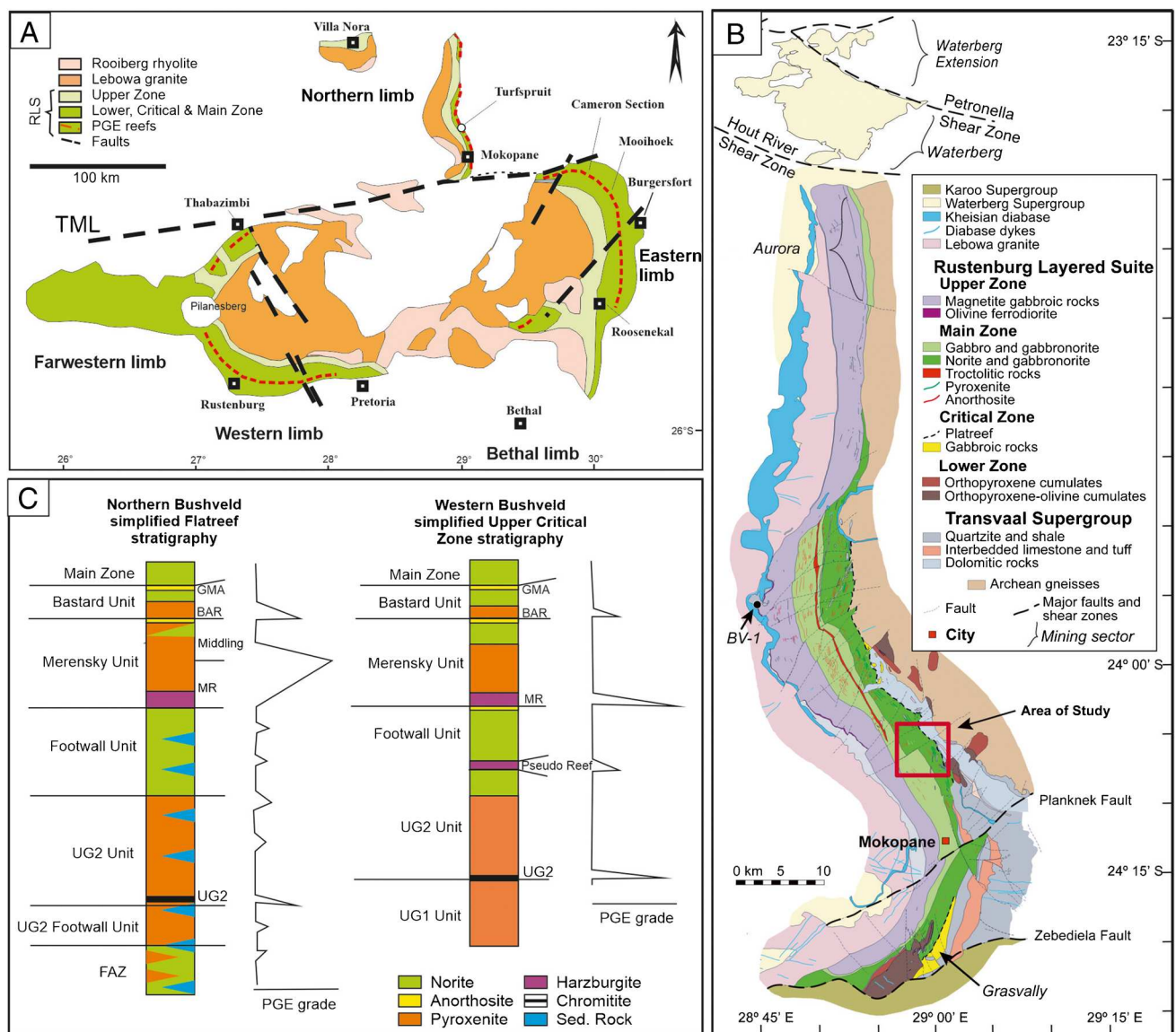


Fig. 1 **A** Geological map of the Bushveld Complex (modified after Maier et al. 2013) showing locality of Turfspruit project. **B** Geological map of Bushveld northern limb (modified after Yudovskaya et al.

2018). **C** Stratigraphy of the Flatreef sequence and correlation with western Bushveld Complex (modified after Grobler et al. 2019)

units: at the top of the UCZ is the Bastard Cyclic Unit. Its uppermost portion consists of a several-m-thick mottled anorthosite correlated with the Giant Mottled Anorthosite (GMA) of the western Bushveld Complex (Grobler et al. 2019). This is underlain by interlayered barren norite and pyroxenite and then PGE-rich pyroxenite, the latter forming the Bastard Reef (BAR in the terminology of Grobler et al. 2019). Next is the Merensky Cyclic Unit. At its top is poorly mineralised or barren norite and/or pyroxenite (termed the Middling in the mine). This is typically underlain by medium-grained mineralised pyroxenite (termed M2), a Cr stringer, a layer of mineralised pegmatoidal orthopyroxenite (termed M1_U) and a basal Cr-rich zone that often includes a distinct Cr stringer. The remainder of the drill core intersects the Footwall Unit comprising > 100 m of interlayered gabbro-norite and pyroxenite, locally olivine bearing, containing abundant sedimentary xenoliths.

Methods

Because parts of the mother hole drill core were used for metallurgical test work, initial assaying was restricted to the two deflections (ESM 2-S1). Elements determined included Cr, Ni, Cu, Pt, Pd, Rh and Au, and analytical methods are described in Grobler et al. (2019). In 2017, we additionally determined major element oxides (except for SiO₂), LOI and a range of trace elements, including S, REE, As, Sb, Ba, Sr, Co, Cr, Ni, V, Zn, Pt, Pd, Rh and Au in 25 samples of the TMT006 mother hole (D₀), using the Setpoint laboratory in Mokopane (ESM 2-S2). Information on analytical results of standards, duplicates and blanks is provided in ESM 2-S3.

Micro X-ray fluorescence (XRF) was performed on the Maia Mapper laboratory XRF imaging system at CSIRO Mineral Resources, Clayton, Victoria. Analytical details are described in Maier et al. (2021b).

Element maps of major and minor elements were acquired using two Oxford Instruments X-MaxN 150 mm² silicon drift energy dispersive X-ray spectroscopy (EDS) detectors on a Zeiss Sigma HD field emission scanning electron microscope (FESEM) at Cardiff University, UK. An accelerating voltage of 20 kV was used with a 120 µm final aperture with a nominal beam current of ~1 nA. EDS data was acquired using Oxford Instruments Aztec software with a step size of 10 µs and a dwell time of XX3 µs. To maximise x-ray throughput, a process time of 0.5 µs was used resulting in a deadtime of ~45% and output count rates of approximately 400,000 cps. Element map data were background corrected and pulse pile-up and overlap corrected using in-built Aztec algorithms.

Four samples from D₂ were scanned in 3D using the Zeiss Versa XRM520 3D X-ray microscope installed at the Australian Resources Research Centre (CSIRO Mineral

Resources, Kensington, Western Australia) equipped with a flat panel detector. The instrument was set-up to 160 kV, 10 W with 1601 projections recorded over 360° rotation and a voxel size of 22.5 µm. The data were processed following methods described in Godel (2013) and Godel et al. (2013).

Results

Lithologies in the TMT006 drill cores

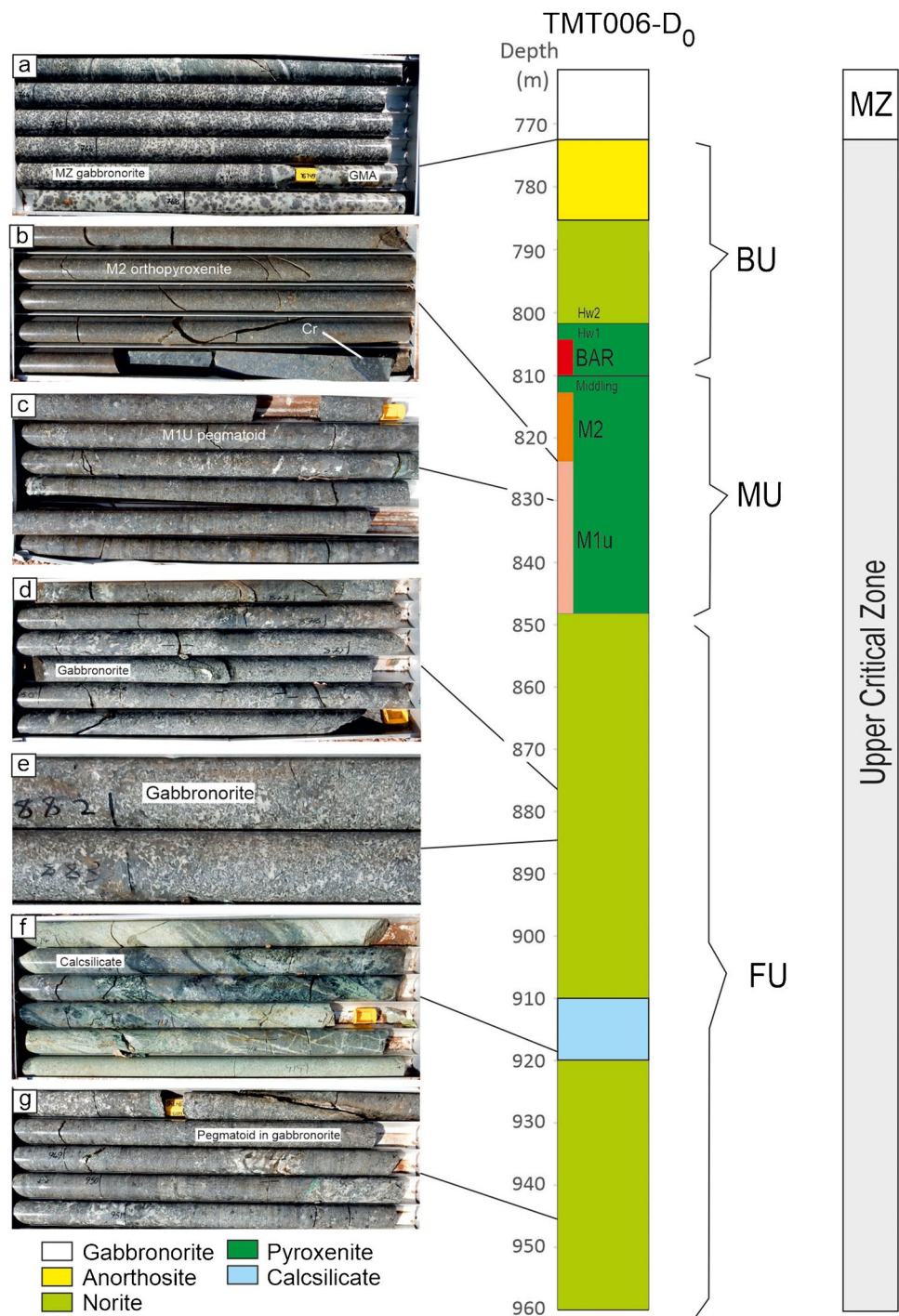
Photographs of drill core boxes containing the complete mineralised interval in TMT006-D₁ are provided in ESM 1-S2, while detailed features of specific layers (mostly from D₀) are shown in Fig. 2. We sub-divide the sequence into cyclic units which typically comprise a basal ultramafic layer (chromitite or pyroxenite) overlain by progressively more evolved rocks including norite, leuconorite and, often at the top of units, anorthosite. Units may be incomplete, with the more evolved portions missing.

The uppermost ~800 m of the TMT006 drill cores intersect the Main Zone (MZ) consisting mostly of poorly layered gabbro-norite, but with a few anorthositic and melagabbro-noritic marker layers in the lower portion (Grobler et al. 2019). In addition, there are a number of cm-to dm-scale lenses of melagabbro-norite and pyroxenite. The base of the MZ is at 767.4 m (D₁), defined by a sharp contact between medium-grained MZ gabbro-norite and underlying UCZ mottled anorthosite (Fig. 2a).

The uppermost unit of the UCZ is the Bastard Cyclic Unit (BCU). It comprises three sub-units. At the top is the above mentioned coarse grained mottled anorthosite (Fig. 2a) constituting hanging wall (HW) 2. The anorthosite is interpreted to represent the stratigraphic correlative to the GMA (Mitchell and Manthree 1992; De Klerk 1992). The layer is unusually thick in TMT006, measuring ~18 m, including a ~5-m-thick medium-grained gabbro-norite layer at about mid-level. The lowermost 20 cm of the GMA show a reduction in grain size. It is underlain, with a sharp contact, by HW 1 comprising interlayered leuconorite, pyroxenite and mottled anorthosite (Fig. 3a). Contacts between the various rock types can be sharp or gradational. At the base of the BCU is a thick, medium-grained orthopyroxenite. Its uppermost ~2.5 m are unmineralised, with the remainder forming the Bastard reef. In the present paper, PGE reefs are defined as having PGE contents exceeding 1 ppm, which means that in D₁ the Bastard reef extends from 802.3 to 816.4 m.

Specific note is made of two narrow (1 cm) bands of leuconorite or anorthosite occurring towards the top of the Bastard pyroxenite (at 801.65 m in D₀) (Fig. 3a, b). The bands show irregular, mushroom-shaped upper contacts, and planar lower contacts. Similar features, resembling load cast

Fig. 2 Lithological log of the analysed Flatreef drill core, complemented by photographs of key lithologies. **a** Basal contact of MZ exposing Giant Mottled Anorthosite at top of Upper Critical Zone, overlain by MZ gabbronorite, TMT006-D1, 767.4 m. **b** Cr stringer at base of medium-grained M2 pyroxenite, TMT006-D0, 821.2 m. **c** M1U pegmatoid orthopyroxenite, TMT006-D0, 826–831 m. **d** Heterogenous gabbronorite and pyroxenite interval in FW3, TMT006-D0, 876.5–882. **e** Varied-textured gabbronorite in FW3, TMT006-D0, ~882–883 m. **f** Calcsilicate, TMT006-D0, 914–919 m. **g** Pegmatoidal pods in FW3 melagabbronorite, TMT006-D0, ~947–951.5 m. Red, orange, and pink bars at left side of stratigraphic column indicate the PGE-enriched intervals: BAR = Bastard Reef, M2 = medium-grained upper part of Merensky Reef, M1U = pegmatoidal lower part of Merensky Reef



structures were observed at the same stratigraphic level in drill cores UMT064 and AMK005, the latter on the farm Macalacaskop. In the remainder of this paper, the layers will be referred to as “mushroom anorthosites”.

The next unit is the Merensky Cyclic Unit (MCU). In most parts of the farm Turfspruit, MCU contains an upper, barren portion termed the “Middling”, consisting of low-grade or barren pyroxenitic, noritic and anorthositic rocks. In the TMT006 holes, the Middling lacks norite and anorthosite,

whereas the pyroxenite is of highly variable thickness, being 1 m thick in D₁ (at 813.4–818.5), but 9 m in D₂ (in D₀ the assaying density is too low to ascertain the precise thickness of the Middling). Thus, in the TMT006 holes the MCU is truncated. The barren pyroxenite of the Middling is underlain by mineralised, mostly medium-grained pyroxenite (818.5–820.4 m), containing a 10 cm pegmatoidal lens near its base (Fig. 2b). The pyroxenite forms the upper portion of the Merensky Reef, termed M2. Next is an approximately

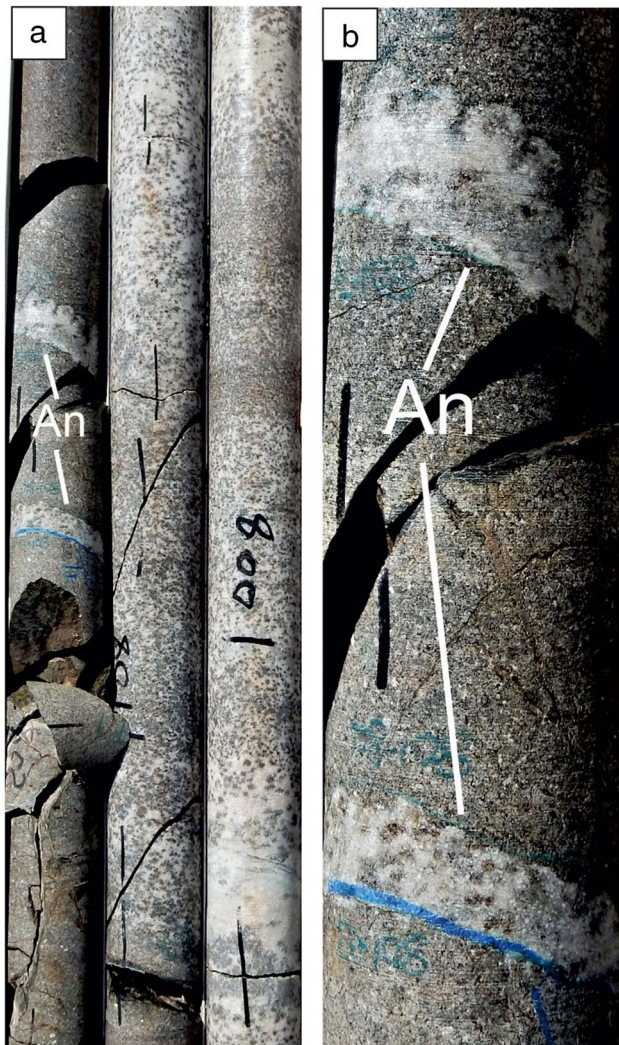


Fig. 3 **a** Leuconorite/anorthosite layers with mushroom-shaped extensions into hanging wall pyroxenite, Bastard cyclic unit, ~10 m above Bastard Reef, drill core TMT006-D0. **b** Close-up of **a**. Width of drill core = 6.4 cm

20-m-thick, PGE mineralised, predominantly coarse grained or pegmatoidal websterite (820.4–843.8 m in D_1), constituting the lower portion of the Merensky Reef, termed $M1_U$ (Fig. 2c). It contains several cm- to dm-sized xenoliths of highly altered metasediment. In many drill cores on the Turfspruit property, the base and top of the pegmatoid are defined by Cr stringers (Grobler et al. 2019), but in TMT006, only the 2–3-cm-thick upper Cr stringer is well defined (Fig. 2b), whereas the basal Cr stringer is irregular and diffuse.

The Footwall Unit (FU) comprises the rocks from the base of the Merensky cyclic unit (~843.8 m in D_1) to the end of the bore hole (~900 m in D_1 , 955 m in D_0). Grobler et al. (2019) distinguished three sub-units (FW1–3) within the FU, based on lithology rather than stratigraphic position.

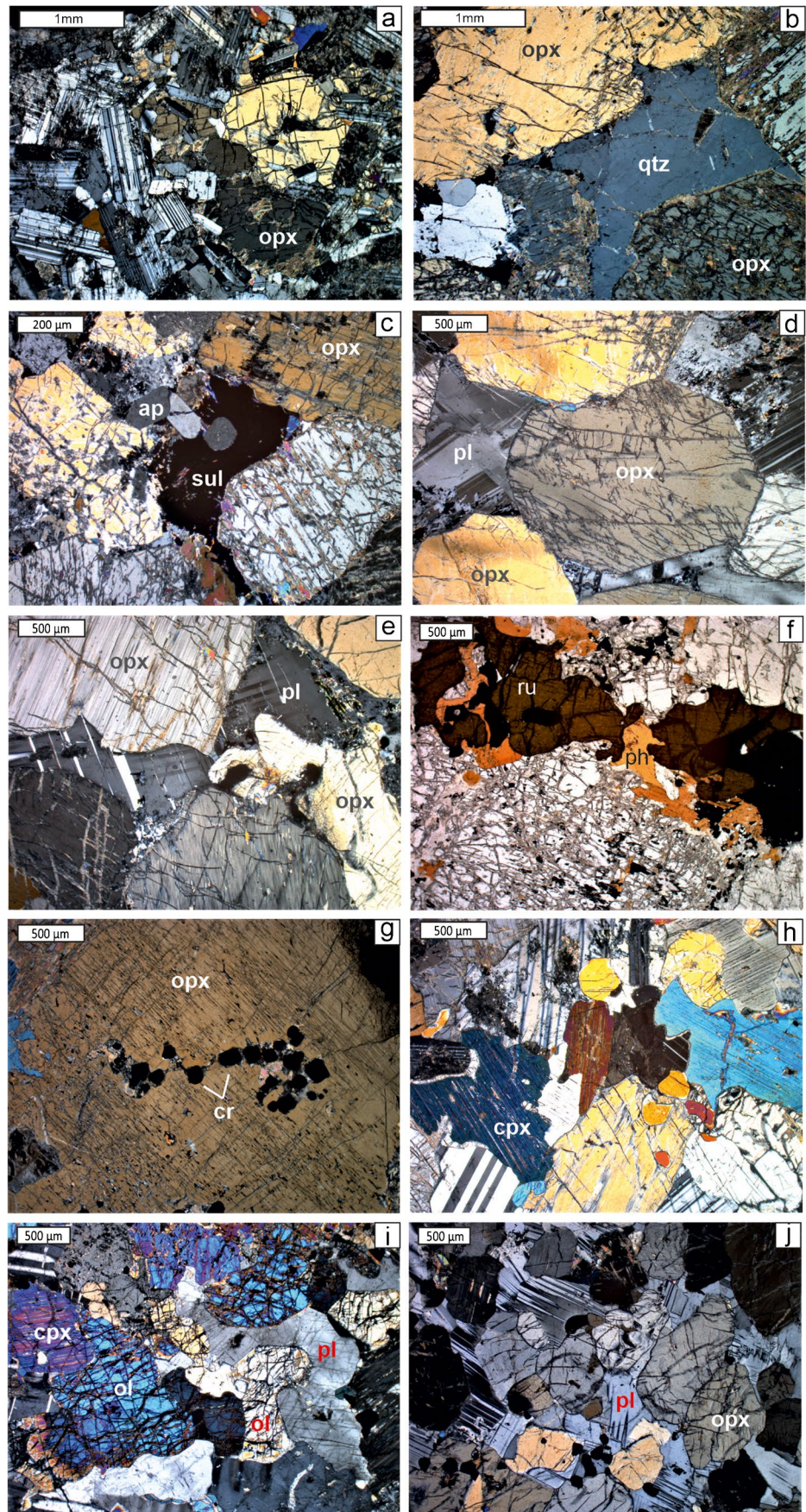
FW1 comprises calcisilicate-contaminated rocks, FW2 is shale-contaminated rock, and FW3 comprises interlayered, relatively poorly contaminated, norite-pyroxenite (Fig. 2d, e, g). In drill core TMT006- D_0 , FW1 is represented by heterogeneous pyroxenites from 843.8 to 877.8 m (Fig. 2d), showing variable grain size and mineral modes. The rocks are enriched in clinopyroxene, contain lenses of massive, patchy and veined serpentinite and show abundant tremolite and talc alteration. Traditionally, such rocks have been informally denoted parapyroxenites in the northern Bushveld. An interval of massive calcisilicate with several large (up to 10 cm) massive and semi-massive sulfide lenses occurs in D_0 from 893.2 to 919.1 m (Fig. 2f, ESM 1-S3 and 4). There is no clear FW2 in any of the TMT006 drill cores. In contrast, FW3 is well developed, consisting of medium-grained to coarse grained norite, gabbronorite and pyroxenite making up lenses and layers within FW1 (e.g. 870.6–872.8 m) and most of the sequence from 877.8 to 893.2 m and from 919 m to the end of the borehole. FW3 contains several pegmatoidal pods which tend to contain elevated sulfide contents (Fig. 2e, ESM 1-S4). The gabbronorites and norites may show textural evidence of disequilibrium crystallisation such as acicular grain shapes and irregular indented and interpenetrating grain boundaries (Fig. 2e).

Petrography of the mother hole (D_0)

Bastard cyclic unit

The main mineral in the medium-grained leuconorite of HW1 (Fig. 4a) is plagioclase. The mineral makes up ~90 modal % of the rock, forming subhedral grains, mostly up to 2 mm in length, that show a subtle fabric normal to the vertical axis of the drill core. Many grains are strongly zoned and show tapered and bent deformation twin lamellae. Grain boundaries tend to be highly irregular and interpenetrating, suggestive of dynamic recrystallisation. The grains are variably sericitized and locally replaced by brown mica. Orthopyroxene forms anhedral grains up to ~3 mm in diameter making up ~10% of the rock. Many grains are partially uranised or altered to talc. Strongly rounded and, sometimes, irregularly embayed plagioclase inclusions occur predominantly within the outer zones of orthopyroxene. Clinopyroxene is a minor phase (<10 modal %) forming large (up to 5 mm wide) oikocrysts. Poorly deformed quartz, showing only moderate undulous extinction, as well as small (<0.5 mm) grains of carbonate and apatite may occur in the interstitial space. In places, the rock contains very fine-grained (<0.1 mm) disseminations of chalcopyrite, typically in interstitial domains. Small pyrrhotite grains with pentlandite exsolution flames may rarely occur along the grain boundaries of some orthopyroxenes. Small anhedral oxide grains, likely magnetite, also occur.

Fig. 4 Photomicrographs of silicate minerals. **a** Leuconorite from HW 1 (sample 799.76). **b** Orthopyroxenite from Bastard reef. Note interpenetrating grain boundaries and weakly undulous quartz. Sample 804.91. **c** Bastard Reef. Note interstitial sulfide associated with apatite. Sample 804.91. **d** Orthopyroxenite from M2 reef. Note deformation of orthopyroxene and plagioclase as indicated by undulous extinction and tapered deformation twin lamellae. Sample 805.97. **e** M2 reef, showing irregular interpenetrating grain boundaries. Sample 807.53. **f** M2 reef, with abundant phlogopite and rutile interstitial to orthopyroxene. Sample 819.89. **g** Orthopyroxenite of MIU unit, with abundant chromite grains within large orthopyroxene grain. Sample 845.4. **h** Gabbro within FW3 unit. Sample 889.15. **i** Olivine norite within FW1, sample 932.63. **j** Melanorite within FW3, sample 937.7



The mushroom anorthosite shown in Fig. 3a has been studied in more detail, using microXRF and FESEM element maps (Fig. 5). These indicate that the hanging wall pyroxenite to the anorthosite contains more chromite and zircon than the footwall pyroxenite and is relatively Fe enriched, particularly in a narrow contact zone directly above the anorthosite (Fig. 5a,b). This contact zone has a markedly lower proportion of interstitial material. The anorthosite contains leuconoritic as well as anorthositic domains, with anorthosite forming corona structures. Plagioclase in the cores of the mushroom structures tends to be relatively Sr rich (Fig. 5c) and, in places, is aligned sub-parallel to the margin of the mushroom head (Fig. 5d). Most of the grains display oscillatory zoning with relatively calcic cores and Na-rich rims. Notably, many of the anhedral pyroxene grains in the rock are surrounded by domains of relatively Ca-enriched plagioclase (Fig. 5d).

The Bastard Reef (BAR) is a sulfide-bearing, chromite-poor orthopyroxenite. Orthopyroxene forms medium-grained subhedral or euhedral grains (up to ~5 mm in width) constituting ~80–90% of the rock (Fig. 4b, c). The grains may show irregular boundaries, being locally embayed by plagioclase suggestive of dynamic recrystallisation. Orthopyroxene contains fine lamellae and blebs of clinopyroxene and is moderately altered to brown mica, talc, uraltite and, locally, antophyllite. Orthopyroxene contains clusters of small subhedral plagioclase inclusions. However, the bulk of plagioclase in the rock, making up ~10 modal %, forms interstitial grains up to ~4 mm in width. Additional phases include interstitial quartz (Fig. 4b, up to ~3 mm) constituting up to several modal % of the layer, particularly in its upper portion, as well as fine-grained quartz intergrowths rimming sulfides. Subhedral clinopyroxene (up to ~1 cm in width) constitutes up to ~5 modal % of the layer, particularly in its lower portion, forming large grains that contain resorbed orthopyroxene chadacrysts. Brown mica (up to several modal %, notably at the base of the layer) may form intercumulus grains associated with quartz, or it may replace orthopyroxene. Apatite (< 1 modal %) forms subhedral grains (up to 2 mm) in the interstitial space (Fig. 4c), containing rare inclusions of zircon. Apatite may be surrounded by a fine-grained mass of an unknown phase (possibly graphite) and is typically associated with quartz, phlogopite and, in some cases, rutile forming few up to 1-mm-sized grains (e.g. at 807.53 m). Sulfides constitute up to 6 modal % of the rock. They consist mostly of interstitial pyrrhotite and pentlandite, broadly in relative proportions of 2:1 but showing significant variation. Chalcopyrite forms minor grains at the margins of pyrrhotite and pentlandite. In addition, fine-grained sulfides (mostly chalcopyrite) occur along grain boundaries between orthopyroxene and other minerals and within interstitial plagioclase (Fig. 6a, b). In general, the rock is strongly altered, mainly affecting plagioclase which

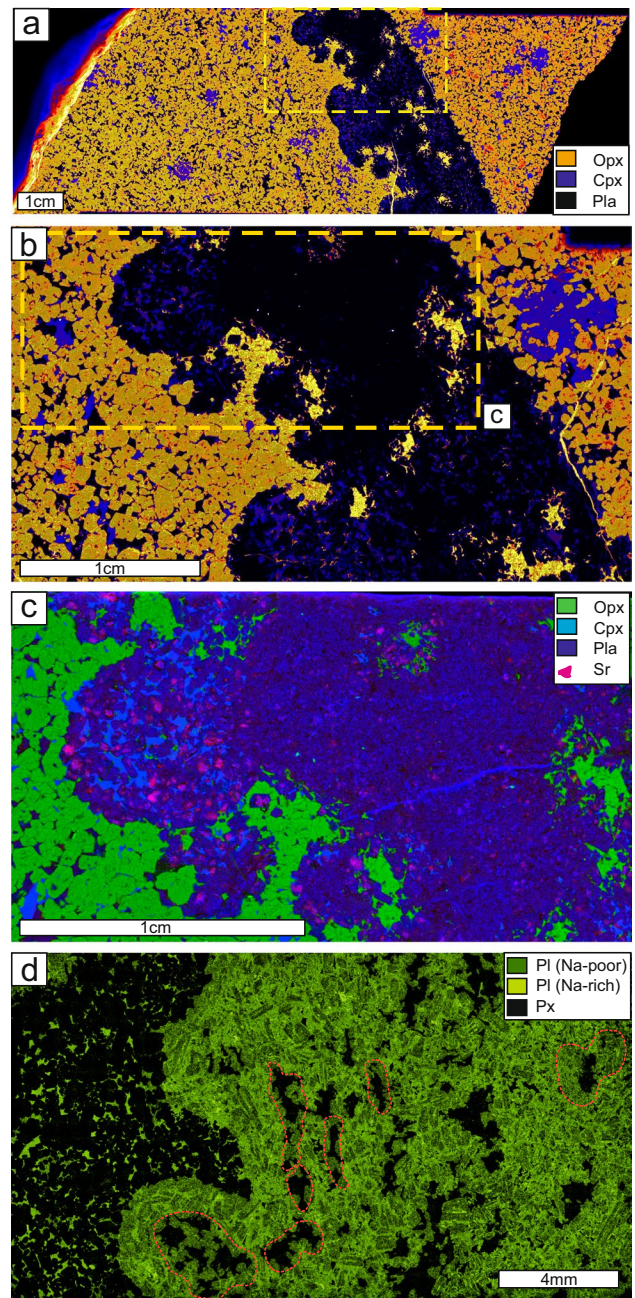
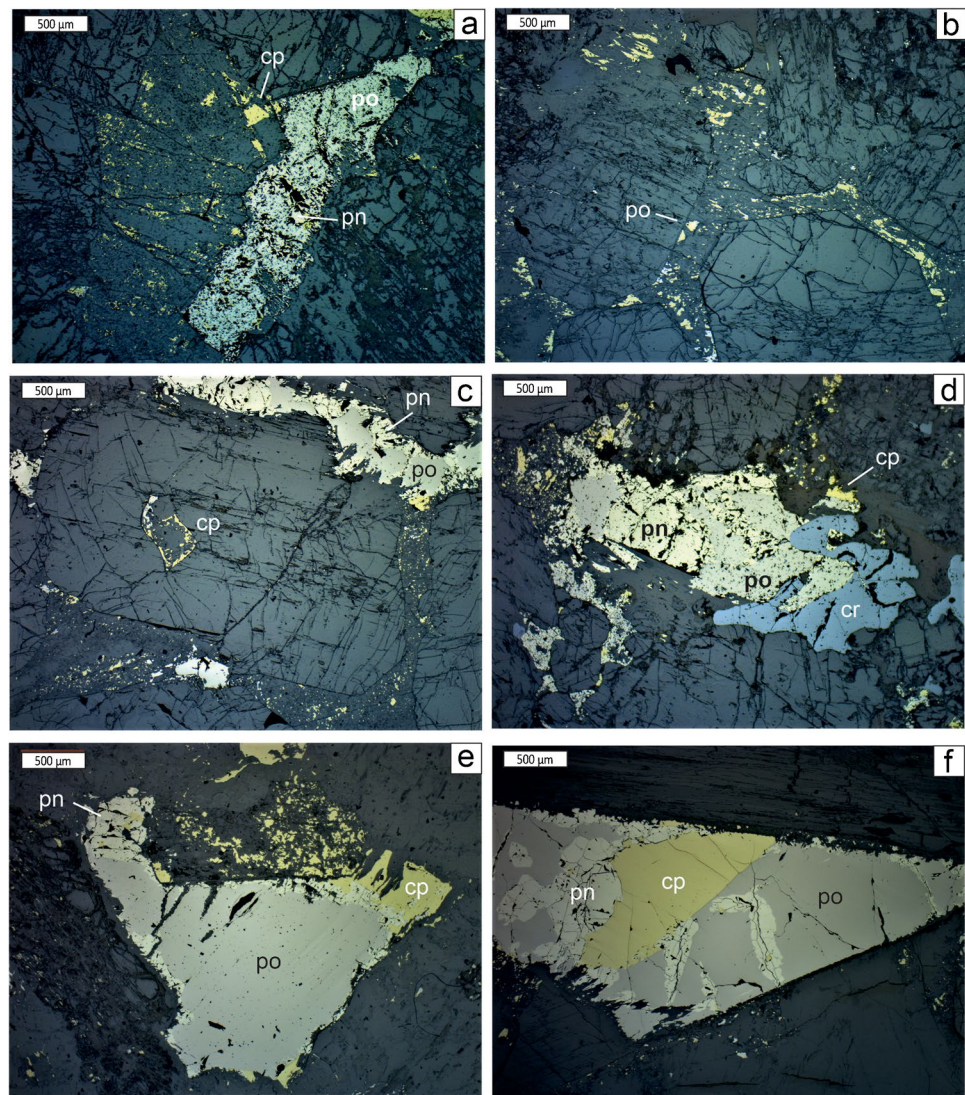


Fig. 5 Element maps of Mushroom anorthosite horizon in Bastard Cyclic Unit HW1 (D0 801.65). a–c were generated by microXRF, d was generated by FESEM. **a** Map of Fe content. Polygon with stippled outline denoted area shown in b. Stratigraphic up is towards left. Note domain of near monomineralic, relatively Fe-rich pyroxenite, shown by relatively light orange colour, above the mushroom layer. **b** Close-up of a, showing relative Fe enrichment in orthopyroxene immediately above and within mushroom layer. For legend, see Fig. 5a. **c** Close-up of b, showing Sr enrichment of plagioclase in upper portion of mushroom layer. **d** Na-map, (AMK005 60.4m) showing that plagioclase tends to display complex zoning, typically with relatively Na-poor cores and Na-rich rims. Also note low-Na domains around pyroxene (indicated by stippled outline) and alignment of plagioclase along the upper margins of the mushroom structures

Fig. 6 Reflected light photomicrographs. **a–b** Orthopyroxenite of Bastard reef, sample 804.91, showing fine-grained chalcopyrite replacing intercumulus plagioclase. **c** M2 orthopyroxenite, sample 813.41, showing vein of massive pyrrhotite with pentlandite concentrated along the margins. **d** M2 orthopyroxenite, sample 819.89, with large grain of po-pent, intergrown with anhedral, vermicular chromite. **e** FW1, sample 856.02, showing composite po-pn-cpp grain with pentlandite concentrated along the margins and chalcopyrite replacing gangue. **f** FW3, sample 942.78, showing composite po-pent-cp grain, with pentlandite forming along cracks and along the margins of the grain



is replaced by sericite and orthopyroxene which is replaced by uralite and, in places, recognisable tremolite and anthophyllite crystals. The rock also shows some evidence for deformation in the form of bent twin lamellae in plagioclase.

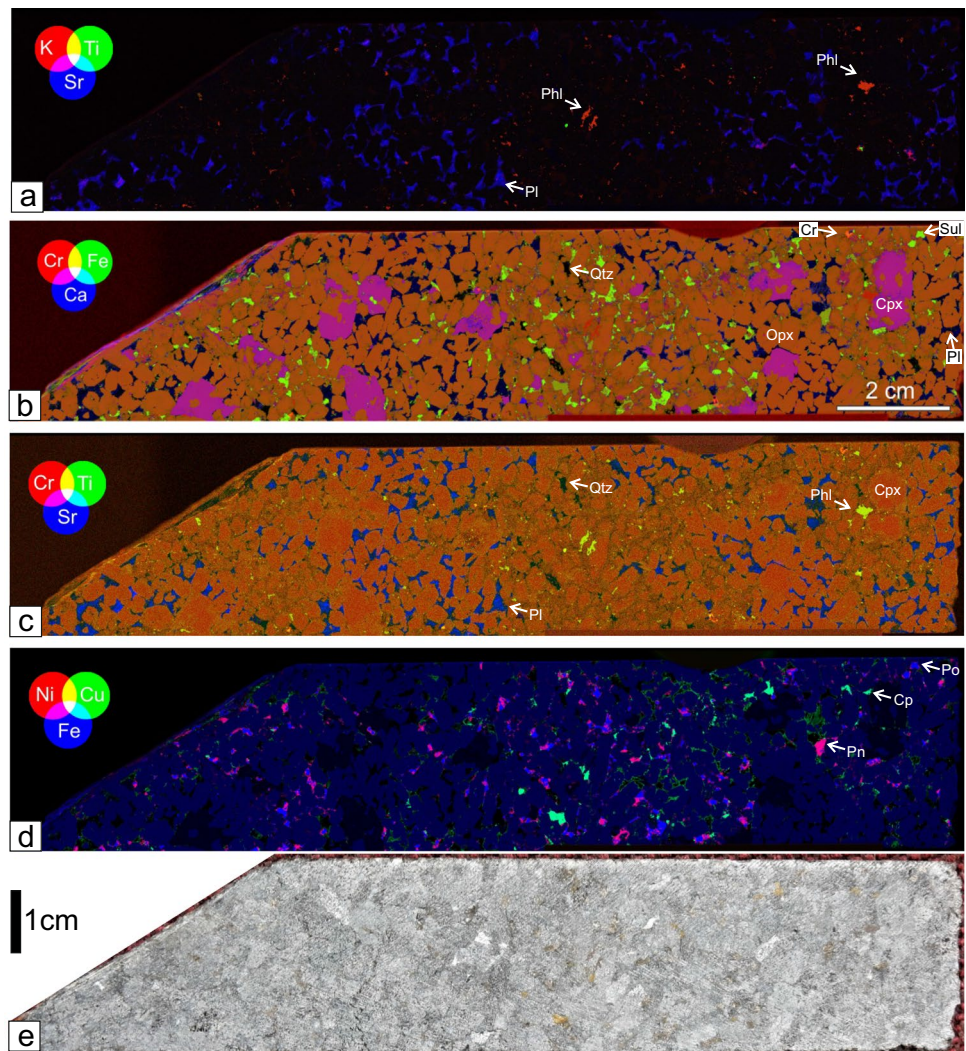
Merensky cyclic unit (MCU)

In D_0 , the Middling is not recognised and BCU is thus directly underlain by MCU. The M2 sub-unit of the MCU consists of sulfide-bearing, medium-grained orthopyroxenite that is somewhat more chromite rich, and markedly more clinopyroxene rich, than BAR. The main mineral is subhedral orthopyroxene (~80 modal %, up to ~5 mm in size), locally interpenetrated and corroded by plagioclase (e.g. at 819.89 m) and containing clinopyroxene exsolution lamellae and blebs (Fig. 4d, e). The orthopyroxene is locally pervasively altered to tremolite and uralite. Plagioclase (~10 modal %) forms interstitial grains up to 2 mm wide

characterised by bent and tapered deformation twin lamellae (Fig. 4d, e). Some samples (e.g. 817.24 m) contain several % interstitial quartz, whereas others contain relatively little quartz (e.g. 813.41 m). Brown mica contents are equally highly variable (Fig. 4f), ranging between <1% to several per cent (e.g. at 817.24 m). Clinopyroxene (~10 modal %) may form large subhedral oikocrysts enclosing orthopyroxene (Fig. 7b). Rutile grains up to >1 mm in size are spatially associated with mica (Fig. 4f). Chromite is rare, except near the base of the unit (819.89 m) where it may form clusters of large sub-rounded and annealed grains (Fig. 4g). Sulfides constitute up to ~4% of the samples, resembling those in BAR, i.e. featuring large grains and grain aggregates of pyrrhotite and pentlandite (Fig. 6c, d), whereas chalcopyrite forms smaller grains located along grain boundaries and within intercumulus plagioclase.

Results of microXRF analysis of a coarse grained orthopyroxenite (sample 818.43 m, Maier et al. 2021b and

Fig. 7 MicroXRF false colour maps of sample 818.43 m, M2 unit, drill core TMT006. **a** K-Ti-Sr map illustrating distribution of plagioclase oikocrysts and concentration of phlogopite and rutile in plagioclase-poor domains, **b** Cr-Fe-Ca map illustrating concentration of sulfides in plagioclase-poor domains, chromite interstitial to orthopyroxene, and large clinopyroxene oikocrysts hosting orthopyroxene inclusions (from Maier et al. 2020). **c** Cr-Ti-Sr map. Note Ti enrichment of rims of orthopyroxene grains and Ca enrichment of cores of interstitial plagioclase, **d** distribution of sulfides. Note interstitial nature of sulfides, as well as occurrence of chalcopyrite along grain boundaries of intercumulus plagioclase. **e** Rock sample



Barnes et al. 2021a, b) are shown in Fig. 7a highlighting that between plagioclase oikocrysts, there are domains that are free of plagioclase. Very fine phlogopite grains are distributed throughout the sample, notably in the plagioclase-free domains where they may be associated with rutile. Orthopyroxene within plagioclase oikocrysts is euhedral or subhedral showing a faint fabric normal to the vertical of the drill core (Fig. 7b). Clinopyroxene forms large (1–2 cm) anhedral to subhedral oikocrysts containing anhedral, sometimes rounded orthopyroxene inclusions. Barnes et al. (2021a, b) interpret similar grains within the Merensky Reef of the western Bushveld Complex as having formed through peritectic replacement of orthopyroxene. Chromite forms mostly very small (<0.1 mm) crystals located within interstitial plagioclase or, to a lesser extent, as inclusions within orthopyroxene chadacrysts hosted in plagioclase oikocrysts. The rock contains several % intercumulus quartz, particularly outside the plagioclase oikocrysts. The sulfides occur in patchy disseminated form, interstitial to orthopyroxene in

plagioclase-free domains where they are in face contact with the cumulus pyroxenes, or in cm-scale domains where all the interstitial space is filled with sulfide separated by patches where none of it is. In contrast, early-formed plagioclase and clinopyroxene oikocrysts are essentially sulfide free. Figure 7c highlights faint zonation of orthopyroxene displaying Ti-rich and Cr-depleted rims. This zonation in orthopyroxene is only evident in monomineralic domains outside the plagioclase and clinopyroxene oikocrysts, suggesting relatively early formation of the oikocrysts preventing further reaction of cumulus orthopyroxene with evolving trapped liquid. Clinopyroxene oikocrysts shows similar zonation from Cr rich cores to depleted rims. This image also provides evidence for zonation of interstitial plagioclase, with elevated Sr and, by implication, An content in the core domains. The proportions of pyrrhotite, pentlandite and chalcopyrite appear to be broadly in the range of typical Merensky Reef sulfide assemblages (50:30:20, see Barnes and Maier 2002) (Fig. 6d). Of particular note is the clear separation

of pyrrhotite and pentlandite from chalcopyrite (Fig. 6a, c, e), suggesting late-stage grain-scale Cu migration into the interstitial space and along grain boundaries. Platinum-rich PGM show a very close spatial relationship to sulfide, being preferentially located a few tens of microns outside, or directly on the edge of sulfide blebs (Barnes et al., 2021b), analogous to what has been observed in the Merensky Reef of the western Bushveld (Li et al. 2004; Prichard et al. 2004; Godel et al. 2007; Smith et al., 2021; Barnes et al., 2021b).

The M1_U sub-unit (Fig. 2) consists predominantly of pegmatoidal websterite. Orthopyroxene is typically ~ 1 cm in size and mostly anhedral but can be locally subhedral or euhedral containing exsolution lamellae and blebs of clinopyroxene, highly irregular inclusions of plagioclase and anhedral but equant inclusions of serpentine and talc that likely represent altered olivine. Orthopyroxene is locally altered to talc and uraltite and may contain serpentine veins. Grain boundaries with other pyroxene and plagioclase grains are highly irregular and interpenetrating. The rock has higher clinopyroxene contents (typically 10–20 modal %) than BAR or M2. Intercumulus plagioclase (up to > 5 mm in diameter) usually forms only a minor component of the rock but can locally make up to ~ 10 modal %. It is locally highly sericitized. Brown mica is not as abundant as in M2 and BAR and mostly of secondary origin, replacing pyroxene. Sulfides typically constitute 2–6 modal % of the rock. They show broadly similar textures as in M2, but composite pyrrhotite-pentlandite grains tend to be larger, and chalcopyrite is less abundant. Pentlandite is concentrated along the boundaries of large composite (pyrrhotite-pentlandite) sulfide grains and locally along fractures. Chalcopyrite mostly forms distinct grains, commonly along grain boundaries of, and fractures within, silicates suggesting late-stage remobilisation, possibly because sulfide melt exsolves an aqueous or halogen-rich vapour phase during the last stages of solidification (Barnes et al. 2021a, b) resulting in migration of Cu into nearby fractures. All sulfides contain abundant needles of tremolite. The basal sample of M1_U (845.4 m) is relatively rich in chromite, consistent with observations from the remainder of the Turfspruit project area (Grobler et al. 2019). Chromite grains tend to form clusters and disseminations that are heterogeneously distributed throughout the rock (Fig. 4g). The grains may be subhedral (mostly 0.1–0.2 mm) or rounded (up to 0.5 mm), or they may form larger annealed grain aggregates (up to 1 mm in width).

In order to further constrain the origin of the sulfide and PGE mineralisation, we analysed four samples of drill core D₂ by high-resolution X-ray computed tomography (Fig. 8, movies in ESM 3). Sample 815.11–815.22 m contained 2.8% sulfides, 823.58–823.68 m contained 6.8% sulfides, 834.92–835.02 m contained 3.0% sulfides and 842.08–842.18 m contained 1.7% sulfides. The samples show large short-range variations in sulfide grain size (with no change in texture) and a relatively

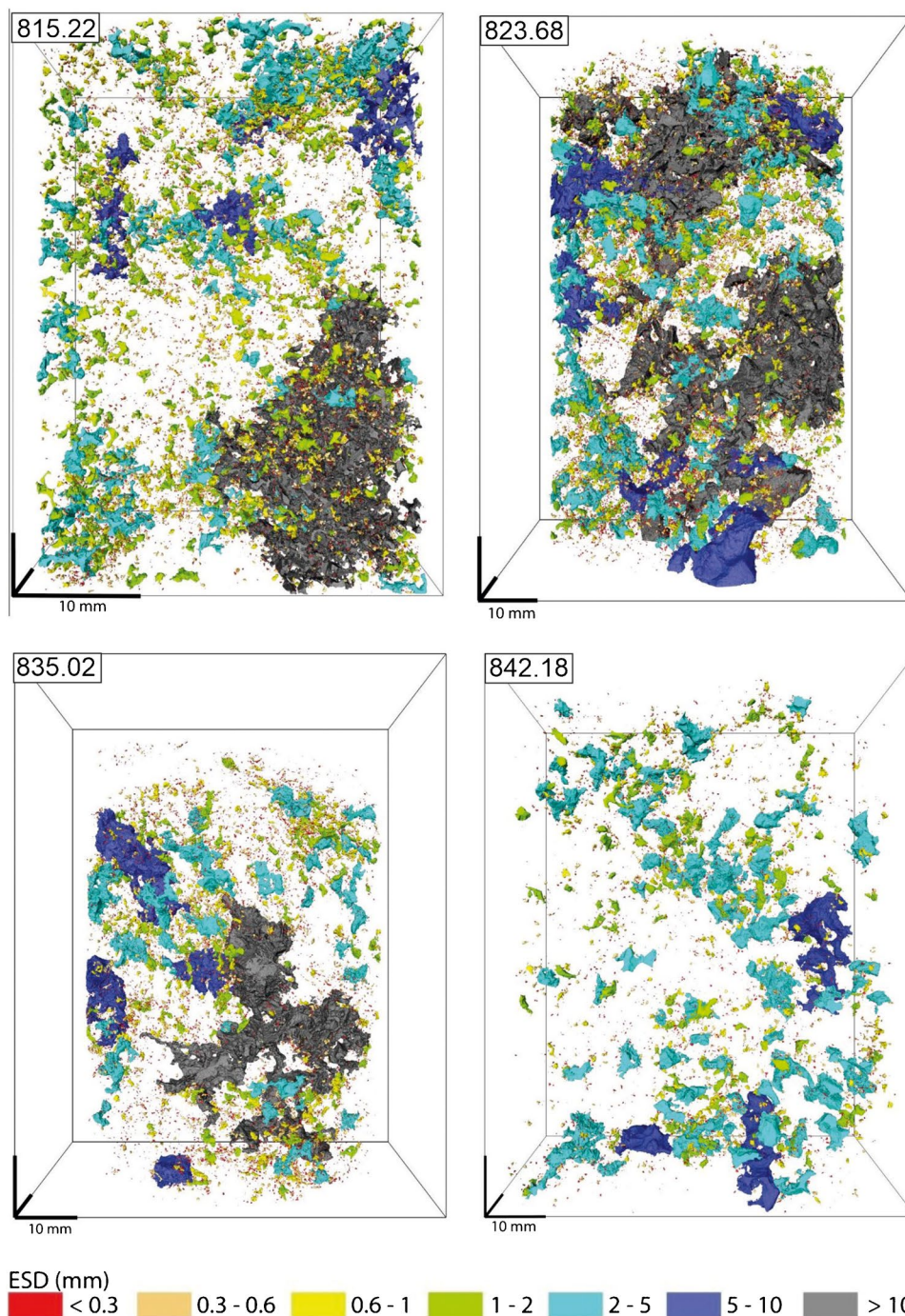
small scale of interconnectivity. Note that few of the blebs (~ 20%, ESM 1-S5a) are larger than ~ 10 mm, but the largest networks extend outside the bounds of the sample and could thus be larger than 10 mm. ESM1-S5b shows a classic crystal size distribution (CSD) plot. The y-axis represents the number of grains per unit volume, normalised to the bin size to allow for the fact that one needs to use larger bins at larger grain sizes. The Y intercept reflects the nucleation rate, i.e. the number of new grains that nucleate per unit volume. The slope reflects the growth rate, suggesting a broadly similar value for all samples. Note, however, that the CSD lines for all samples are somewhat curved, possibly suggesting mixtures of different grain size populations.

We have also captured the distribution of Pt-rich grains (PGM and Pt alloys, Fig. 8, movies in ESM 3). It should be noted that the scans were done at relatively low resolution to image the entire drill core samples; thus, platinum grains smaller than a few microns are not captured. The great majority of the captured grains are < ~ 350 µm (ESM1-S5c). The samples display broadly similar slopes in the plot, except for the uppermost sample (815.22 m) which has a slightly shallower slope, suggesting that the size of Pt grains carrying most of the total mass of Pt is somewhat larger. The CSD plots for all four samples show straight lines (ESM1-S5d) suggesting a homogenous population of growing grains formed in essentially the same way, e.g. via crystallisation from the late-stage fractionation products of the sulfide liquid. The data are inconsistent with multiple populations of early PGMs growing at magmatic temperatures mixed with lower-T PGMs exsolving from solid sulfides as one would expect kinked lines reflecting mixtures of different slopes in that case.

Footwall unit

Footwall 1 has a highly variable composition, comprising calcsilicate contaminated magmatic rocks and intervals of pure calcsilicate several metres in thickness. In comparison to BCU and MCU, the magmatic rocks are generally strongly enriched in clinopyroxene and, locally, olivine, and they tend to be more altered. For example, sample 856.02 m consists of 70% large clinopyroxene grains (1–4 mm), 10–15% orthopyroxene (up to 5 mm), 10% interstitial plagioclase (up to 3 mm), several % sulfides (pyrrhotite, pentlandite and chalcopyrite in broadly similar proportions as in MCU and BCU) and large laths of phlogopite (up to 1 mm, < 1 modal %). Grain boundaries between minerals are irregular and interpenetrative suggestive of dynamic recrystallisation. Alteration minerals comprise tremolite, sericite and uraltite. Other trace phases that are relatively common in the overlying units such as quartz, apatite and rutile are not observed. Some samples (e.g. 861.43 m) contain abundant serpentine in the form of interstitial masses and veins. Yet other samples (e.g. 932.63 m, Fig. 4i) consist of olivine

Fig. 8 High-resolution X-ray computed tomography images of analysed samples. Note that sulfides are colour coded according to size (see ESM 3 for 3D movies). PGM are shown as small red dots



gabbro, containing ~30% cumulus plagioclase, ~40% clinopyroxene, ~10–15% strongly serpentinised olivine, ~5–10% orthopyroxene and small amounts (~1%) of secondary brown mica. Sample 903.12 m contains a massive sulfide bleb, with the silicates being extremely altered to tremolite, uralite and some talc.

Based on textural, mineralogical and compositional data (e.g. low whole rock Ca/Al), Footwall 3 consists of relatively uncontaminated noritic and gabbroic rocks of highly variable grain size (Fig. 2e, g). For example, gabbro-norite

sample 873.54 m has large (> 0.5 cm) orthopyroxene grains (~40–50%) with subhedral or anhedral plagioclase inclusions. The rock is locally strongly uralised and contains abundant tremolite as well as veins of serpentine. Clinopyroxene (~30%) is less abundant than orthopyroxene and forms subhedral grains 1–> 5 mm. Cumulus plagioclase (~25%) is mostly relatively undeformed but forms annealed grains. Brown mica is rare and mostly of secondary origin. In contrast, norite in sample 937.7 m (Fig. 4j) is a medium-grained orthocumulate with abundant (~5%)

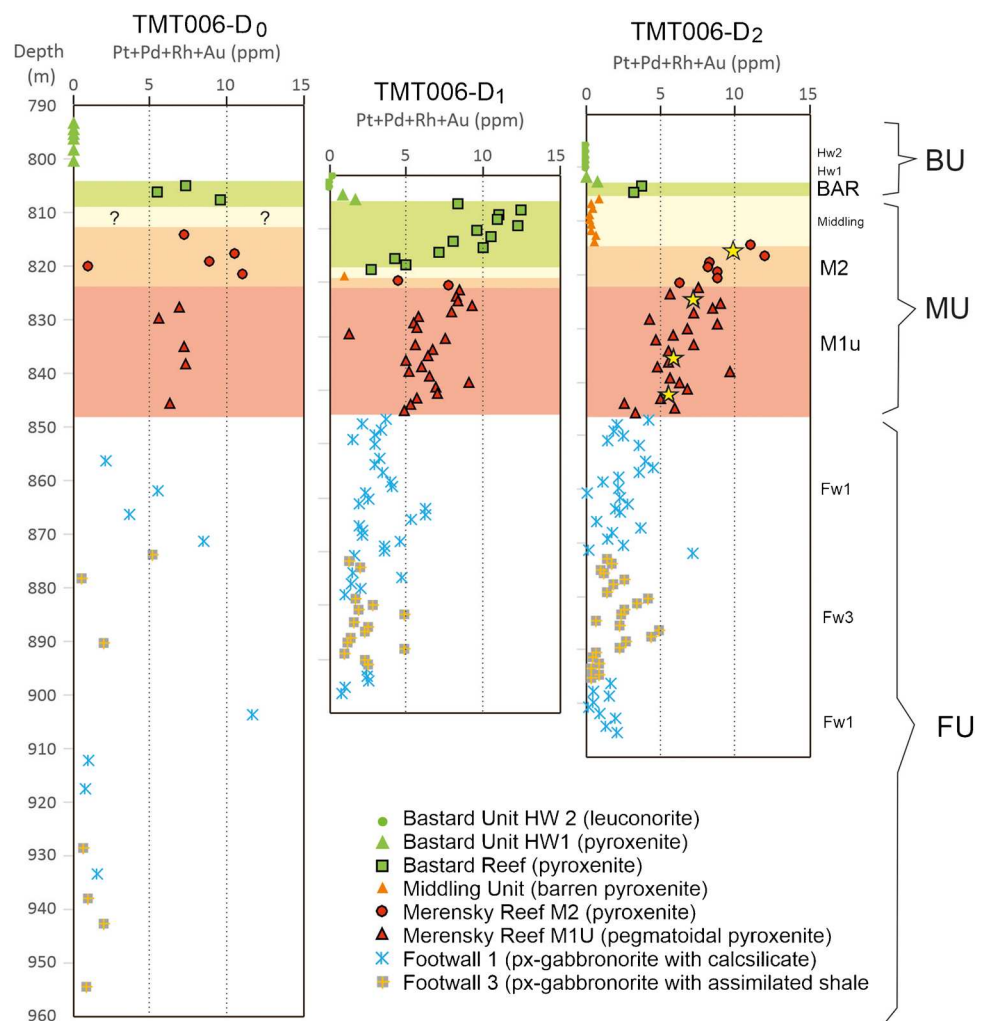
subhedral chromite grains (0.1–0.2 mm) arranged in chains. Orthopyroxene (~60%) forms stubby subhedral grains. Its boundaries to anhedral plagioclase (~20–30%) are highly irregular, indented and interpenetrating, and plagioclase shows undulous extinction and tapered and bent twin lamellae. Anhedral or subhedral clinopyroxene makes up around 5–10 modal % of the rock. Gabbroic samples may be medium-grained (889.15 m, Fig. 4h) displaying equant grains of cumulus clinopyroxene and highly irregular grain boundaries, or they may be coarse grained (938.3 m) and largely altered to tremolite, uralite, sericite and serpentine. Yet other gabbroic samples are pegmatoidal (954.1 m).

Whole rock geochemistry

Assay data on a 1 m scale for Pt, Pd, Rh and Au (4PGE) indicate that the total thickness of the main mineralised interval, i.e. from the top of the Bastard Reef to the base of the Merensky Reef, and the location of its upper boundary, are broadly

similar in the three examined drill cores (Fig. 9). In contrast, some of the individual layers, notably the Bastard Reef, the Middling and M2, show strong variation in thickness and grade between the drill cores. For example, in TMT006-D₂, BAR forms a relatively thin (~2 m) PGE-enriched layer containing ~3–4 ppm 4PGE separated from the Merensky Reef by several metres of poorly mineralised or barren rocks of the Middling. In TMT006-D₁ BAR is much thicker (12 m), its grade is much higher (up to 12.5 ppm 4PGE), PGE contents progressively decrease with depth, and the Middling is much reduced in thickness. M2 is significantly thinner in D₁ than in the other two drill cores (Fig. 9). It thus appears that the thicknesses of BAR and the combined package of Middling and M2 are complementary; where BAR is thick, the Middling + M2 are thin, and vice versa. The FU is best represented in D₀ where it consists of ~100 m of interlayered FW1 and FW3. In contrast, in D₁ and D₂, only ~50 m of FU is intersected before the end of the bore hole. However, assaying density is much higher in the deflections.

Fig. 9 Comparison of PGE contents in the TMT006 drill cores. Star symbols in D2 denote samples analysed by CT scans



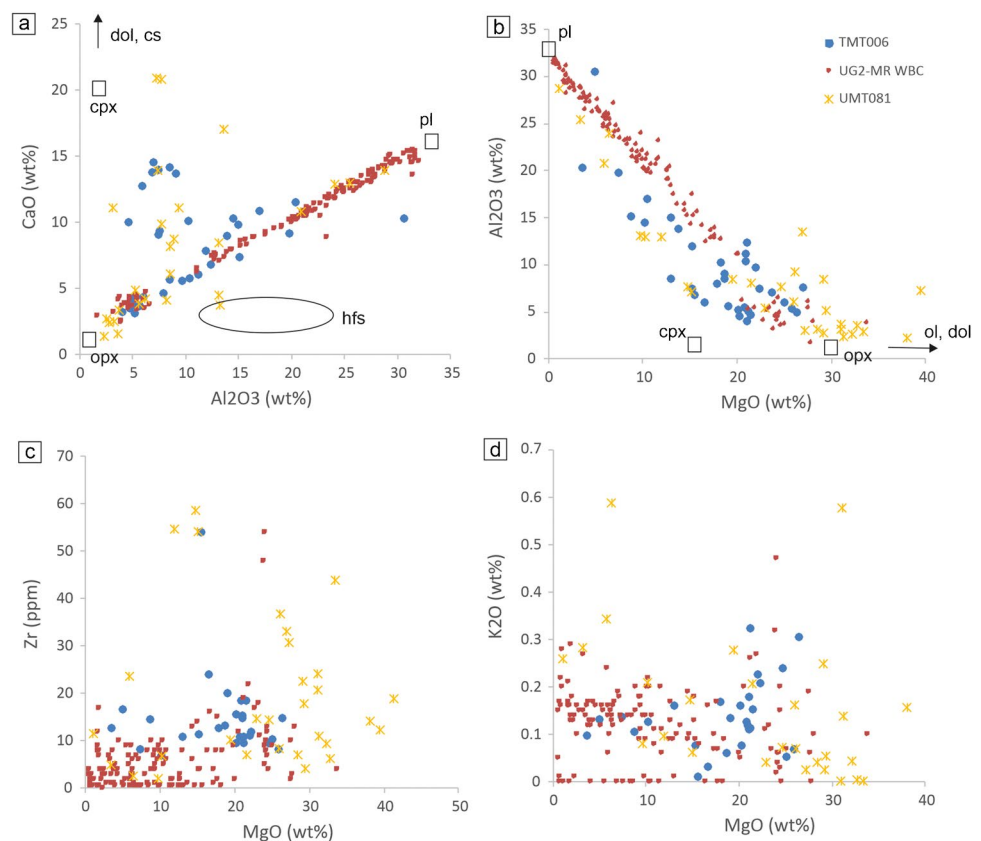
Of particular note is the broad downward decrease in PGE contents, both within individual units such as BAR in drill core D₁, but also across the whole sequence, from > 10 ppm 4PGE in BAR to as little as 0.5–1 ppm in the lower portions of FU. This decrease in PGE is matched by a decrease in the proportion of sulfides (ESM1-S6), from as much as ~6% in BAR to mostly 1–2% at the base of FU, with the exception of some relatively small pods and layers of massive sulfide in the latter. In contrast, Pt/Pd and Au/Pd show less variation in the bulk of the sequence (ESM1-S6), except for progressively lower Pt/Pd in the deeper portions of the Footwall Unit (not exposed in D₁, but clearly evident in D₀, ESM1-S7) and markedly elevated Pt/Pd and Au/Pt in the uppermost Flatreef (M2 and BAR). Cu/Pd is > 10,000 in the HW units (i.e. significantly above primitive mantle values of ~7000), but mostly around 1000 in MCU and BCU, and slightly higher than that (~1500) in the lower portion of FU. Cu/Ni is largely constant in much of the sequence, but with some higher values in FU.

The compositional variation in a range of lithophile elements and element ratios, determined in D₀, is shown in ESM1-S7. The Al₂O₃ contents of the rocks serve as a broad measure of the modal proportion of plagioclase, being relatively low (< 10 wt.%) in the reef interval, but mostly > 10 wt.% in the hanging wall rocks of the reef interval and in FW3. Analogous to many other drill core

intersections from the Turfspruit project area, the pyroxenites of BCU and MCU have relatively constant Cr contents of ~1000–2000 ppm, suggesting that Cr is mainly controlled by orthopyroxene, whereas chromite is mostly confined to the intervals around the basal and upper contacts of M1. The rocks have highly variable Cr/MgO, generally > 40 and overlapping with the rocks of the Upper Critical Zone (UCZ) of the WBC (Maier et al. 2013), whereas typical Bushveld MZ rocks tend to have Cr/MgO < 45. CaO/Al₂O₃ in the TMT drill core is strongly dependent on the proportion of clinopyroxene which has CaO/Al₂O₃ ~ 10. In the relatively clinopyroxene-poor magmatic rocks of BCU, MCU and FW3, CaO/Al₂O₃ is thus mostly below unity, similar to UCZ rocks in the WBC (Maier and Eales 1997), whereas in FW1, CaO/Al₂O₃ is between 1 and 2. Ce/Sm in the relatively uncontaminated upper Flatreef is between 5 and 10, in the range of average MZ and UCZ rocks (Maier and Barnes 1998), whereas the FU has mostly lower ratios of ~5.

The major element composition of the TMT006 drill cores is essentially controlled by the relative proportions of orthopyroxene and plagioclase (Fig. 10). However, the TMT006 rocks show significantly more scatter in binary plots of MgO, Al₂O₃ and CaO (Fig. 10a, b) than rocks of the stratigraphically broadly equivalent UG2-MR reef interval in the WBC. In particular, the Flatreef rocks show relative enrichment in CaO and depletion in Al₂O₃ which

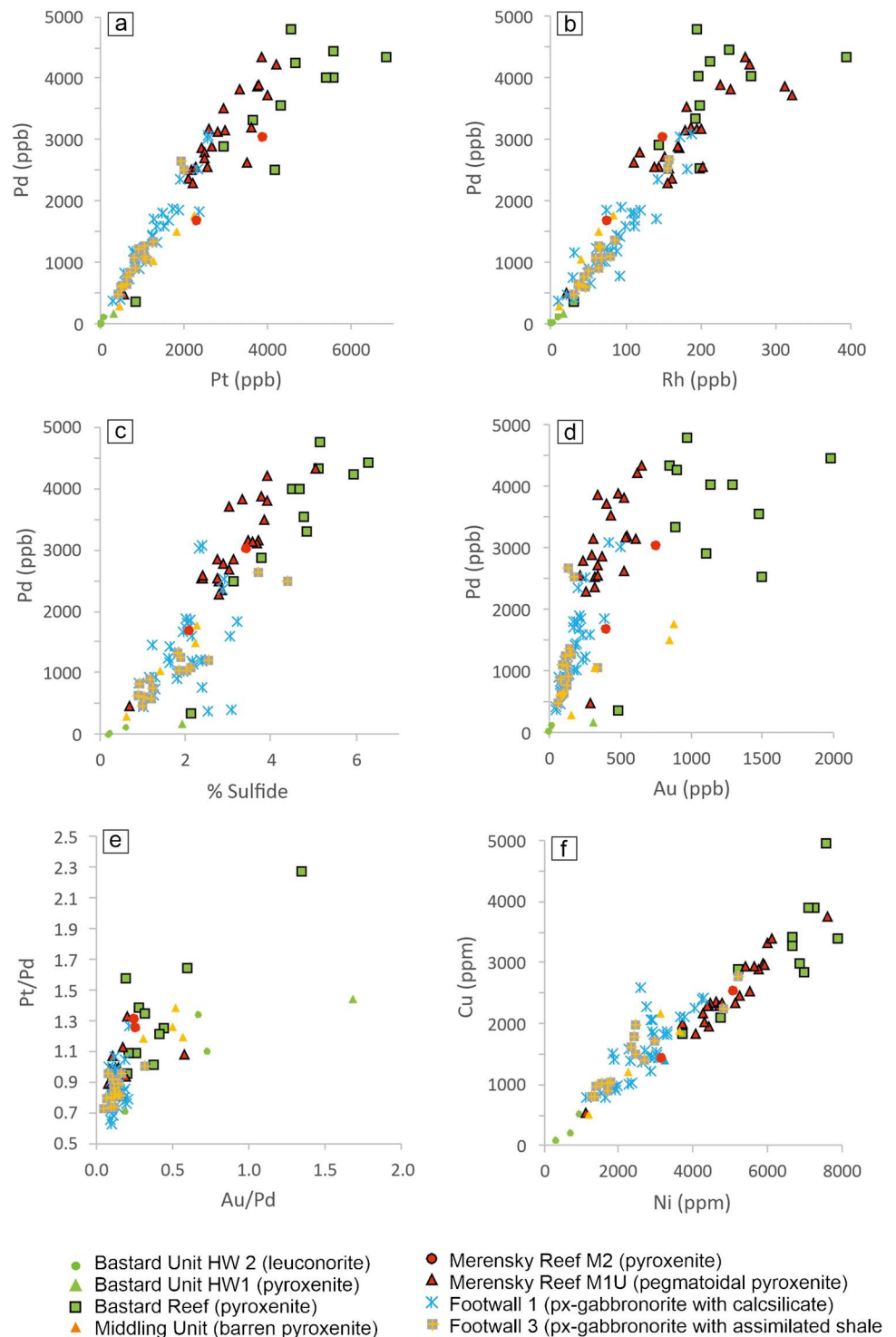
Fig. 10 Comparison of Flatreef rocks to UCZ of WBC. **a** CaO vs Al₂O₃. Note enrichment of Flatreef rocks in CaO. Also note that there is little evidence for hornfels contamination in the Flatreef. **b** Al₂O₃ vs MgO. Note depletion of Flatreef rocks in Al₂O₃. **c** Zr vs MgO. **d** K₂O vs MgO. Note subtle enrichment of Flatreef rocks in Zr and K₂O relative to UCZ of WBC. Data for drill core UMT081 are from Abernethy (2020) and data for UG2-Merensky Reef interval in western Bushveld Complex are from Maier and Eales (1997)



can possibly be assigned to their elevated clinopyroxene content. Incompatible minor and trace elements such as Zr and K_2O do not show significant enrichment in the Flatreef relative to the UCZ of the WBC, except that the Flatreef lacks incompatible-trace-element-depleted adcumulates which tend to be relatively common amongst the norites and anorthosites of the WBC (Fig. 11c-e).

The noble metals show well-defined positive correlations in plots of Pd vs Pt, Pd vs Rh, Pd vs sulfide and Cu vs Ni (Fig. 12), and there is also a good positive correlation between Cu and Ni. The samples from M1, M2 and, particularly, BAR show markedly more scatter in the binary variation plots than those of the other units. The plots also highlight the relatively elevated Pt/Pd of BAR, seen across

Fig. 11 Binary variation diagrams of chalcophile metals and metal ratios in the units of the Flatreef. **a** Pd vs Pt. **b** Pd vs Rh. **c** Pd vs % sulfide. **d** Pd vs Au. **e** Pt/Pd vs Au/Pd. **f** Cu vs Ni



the property (Grobler et al. 2019; Maier et al. 2021a, b). Gold contents of BAR also show enrichment relative to Pd, as indicated by high Au/Pd (ESM1-S6, Fig. 11d). In addition, Au is also enriched relative to Pt, as suggested by high Au/Pt ratios in the unit (not shown).

Lateral variation in metal grade

The lithological units of the Flatreef show considerable lateral continuity (Grobler et al. 2019), but the amounts of sulfide and PGE within units can be highly variable. Thus, adjacent to the high-grade TMT006 intersections, there are drill core intersections that may have less than 50% of the TMT006 PGE budget (ESM 1-S1b). This is a major difference to the Merensky Reef of the western and eastern Bushveld Complex which shows largely continuous grade along strike, except for potholes (e.g. Viljoen et al. 1986).

Discussion

Comparison of mineralisation in the Flatreef and the UCZ of the western Bushveld Complex

To better understand the origin of the Flatreef mineralisation, we compare the rocks to the Platreef and the Merensky Reef in the western Bushveld Complex (WBC) with which the Flatreef has been correlated by Grobler et al. (2019) (Fig. 12). The uppermost portion of the Flatreef shares certain compositional features with the WBC Merensky Reef, notably the sulfide content of the rocks (up to ~6%; Fig. 12a), but the WBC Merensky Reef tends to have higher Pt/Pd (Fig. 12b), Pt/Au (Fig. 12c) and Pt/Cu (Fig. 12e). In contrast, Pt/Ir of the Flatreef overlaps with the WBC Merensky Reef but is markedly higher than in the Cr-rich UG2 and UG1 units as well as the LCZ and LZ of the WBC (Fig. 12d).

Comparison of metal contents of specific rock types (e.g. ultramafic vs leucocratic rocks) is fraught with uncertainty because the available PGE data of silicate rocks in the WBC are strongly biased towards ultramafic rocks. Nevertheless, Maier and Barnes (2008), Naldrett et al. (2009) and Maier et al. (2013) show that most mafic rocks of the UCZ in the WBC contain 10–20 ppb PGE, i.e. much lower values than in the ultramafic rocks. The mafic rocks of the Flatreef are equally relatively PGE depleted compared to the ultramafic rocks (Fig. 12f), but the trend is somewhat less pronounced than elsewhere in the Bushveld.

The most notable difference between the Flatreef and the UCZ in the WBC is the vastly greater thickness and thus the total amount of sulfide and PGE, in the Flatreef. The TMT006 sequence is one of the thickest reef intersections, containing ~4.5 ppm PGE (Pt + Pd + Rh + Au) over 90 m,

including ~45 m at > 6 ppm PGE (Fig. 9). In addition, the footwall to the main mineralised interval contains a further ~1–2 ppm PGE over 60 m to the end of the borehole. Normalised to 1 m, approximating the typical thickness of the MR in the WBC, the Flatreef in drill core TMT006 contains 411 ppm PGE, as opposed to ~5–6 ppm for each of the MR and UG2 chromitite of the WBC. Thus, there are almost 2 orders of magnitude more PGE in the TMT intersections than in the Merensky Reef of the WBC. A further important feature of the Flatreef is that there are relatively few rocks that have < 100 ppb Pt and Pd each, < 100 ppm Cu and < 1000 ppm S, whereas the majority of samples from the LZ, CZ and MZ of the WBC fall into that category (Fig. 12a, c, f).

Origin of the high PGE and sulfide contents of the Flatreef

(i) In situ assimilation of external sulfide

The conventional view has been that the relatively high PGE and sulfide contents of the northern lobe cumulates result from assimilation of sulfidic country rocks by the Platreef/Flatreef parent magma (Buchanan and Rouse 1984; Barton et al. 1986; Grobler et al. 2019). One of the key arguments is spatial association with sulfidic country rocks: Contrary to the CZ of the western and eastern Bushveld Complex which rests mostly on LZ which in turn rests mostly on quartzite, most CZ magmas of the northern lobe intruded into relatively less refractory rocks, including dolomite, iron formation, sulfidic black shale and granite. For the Flatreef, the case for in situ assimilation of sulfur is particularly strong as it contains more sulfide than most other intrusives of the northern lobe (Kinnaid et al. 2005; Maier et al. 2008) and because it is entirely hosted by the sulfide-rich Deutschland Formation. The sulfide assimilation model is consistent with the available sulfur isotopic data showing strongly positive $\delta^{34}\text{S}$ throughout much of the mineralised Flatreef interval (Yudovskaya et al. 2017; Keir Sage et al. 2021) as well as many Platreef intersections elsewhere in the northern limb (Manyeruke et al. 2005; Holwell et al. 2007; Sharman et al., 2013). In contrast, Holwell et al. (2007) have shown that the uppermost portion of the Platreef has a near-magmatic sulfur isotopic signature, which the authors interpreted to reflect a mantle origin for sulfur. However, Leshner and Burnham (2001) demonstrated that at high mass ratios of silicate to sulfide magma (R factor), any crustal isotopic signatures of the sulfides can be highly diluted.

In Fig. 13, we have modelled R factors applicable to the Flatreef. Barnes and Maier (2002) suggested that the Merensky Reef of the WBC formed from mixed B1 and B2 magma, in the proportion 60:40. Using this estimate for the Flatreef parent magma, the modelled R for the upper Flatreef

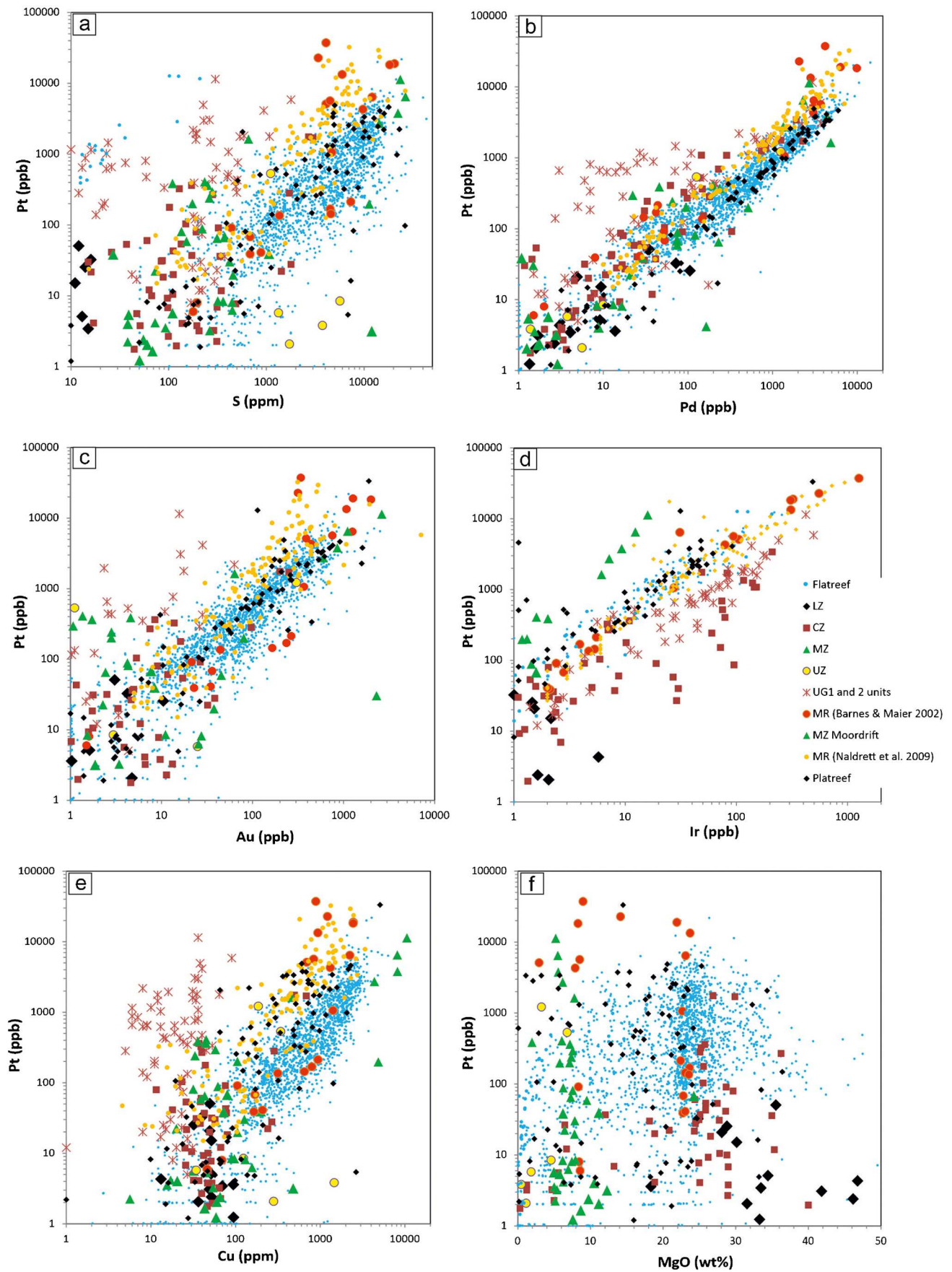


Fig. 12 Binary variation diagrams showing comparative metal contents in Flatreef and UCZ of WBC. **a** Pt vs Pd, **b** Pt vs Au, **c** Pt vs Cu, **d** Pt vs Ir, **e** Pt vs MgO, and **f** Pt vs S. Data sources: LZ, CZ, MZ, and UZ from Maier et al. (2013), Merensky Reef from Barnes and Maier (2002) and Naldrett et al. (2009), UG1-2 from Maier and Barnes (2008), and MZ Moordrift from Maier et al. (2008)

is just above 10,000 (Fig. 13a), consistent with estimates by Ihlenfeld and Keays (2011) for the Platreef. However, modelled sulfide contents for BAR and M1/2 are mostly 5–10, somewhat higher than the observed concentrations. Maier et al. (2021a, b) suggested that in the Flatreef the hybrid B1-B2 magma had assimilated ~90 ppm Cu from the footwall. Using this estimate, *R* factors reach 20,000–30,000, and sulfide contents are 2–5%, broadly in line with observations (Fig. 13b). At such *R* factors, any crustal signature of the contaminated Flatreef magma would be highly diluted; For example, at *R* = 20,000, the original contrast between a pure mantle magma and a crustal sulfide contaminant is reduced by 90–95% (Leshner and Burnham 2001). Sulfur isotopes are thus of limited use in constraining the degree of crustal contamination of the uppermost, most strongly PGE mineralised Flatreef.

The sulfides in the magmatic rocks underlying the Flatreef have strongly positive $\delta^{34}\text{S}$ (Yudovskaya et al. 2017; Stephenson 2018; Keir-Sage et al. 2021). This could suggest that the rocks of the Footwall Units were more contaminated with crustal sulfur. In addition, the equilibration of the sulfide melt with the silicate magma could have been less efficient; *R* factors may have been as low as 1000 for the Footwall Unit (Fig. 13b).

(ii) Entrainment of sulfides from depth

One of the key criticisms of the in situ assimilation model has been that there are few PGE depleted residual rocks in the northern limb. The average Flatreef rocks (Maier et al. 2021b) have at least 20 times the PGE content of the B1 or B2 parent magmas. Thus, the precipitation of 250 m of mineralised rock (Abernethy 2020) would produce ~4 km of PGE depleted residual magma, whereas the Flatreef is overlain by no more than a few 10 s of metres of PGE depleted CZ rocks. The overlying Main Zone is locally cross cutting the Flatreef (Holwell and Jordaan 2006) and has PGE-undepleted Cu/Pd ratios (Maier et al. 2013) and some highly PGE-enriched horizons (Kennedy 2018). The Main Zone is thus unlikely to represent the residual magma to the Flatreef. These observations have led several authors to propose that the Platreef/Flatreef formed from emplacement of metal- and sulfide-charged magmas (Barton et al. 1986; Harris and Chaumba 2001; Maier 2005; Hutchinson and Kinnaird 2005; McDonald and Holwell 2007; Holwell and McDonald 2007; Ihlenfeld and Keays 2011; Beukes et al., 2021).

However, hypothesising about mass balance in layered intrusions is rarely conclusive and difficult to test. For example, one could argue that any PGE-depleted residual magmas moved up-dip or down-flow. Alternatively, the sulfidic cumulates could have been locally thickened due to granular flow. The latter model is consistent with the relatively ultramafic bulk composition of the Flatreef compared to the UCZ of the WBC; Noritic and anorthositic rocks are relatively rare, whereas ultramafic layers are much thicker, frequently in excess of 100 m. They form cumulate piles with remarkably homogenous composition (Maier et al. 2021b), particularly in the large trough-like centre of the Flatreef (Grobler et al. 2019). These data could suggest that the Flatreef formed through hydrodynamic concentration of sulfidic ultramafic rocks in flow dynamic traps, whereas plagioclase would have concentrated near the top of the pile and potentially be eroded by successive ultramafic slurries or the large MZ influx (Maier et al. 2013; 2021b). However, until underground developments allow documentation of potential features such as grain lineation, grain-size sorting and trough banding, testing of this model remains difficult.

Another argument in support of sulfide entrainment is the high metal tenor of the Flatreef sulfides, suggesting high *R* factors (Fig. 13). If it is assumed that basaltic magmas become sulfide saturated at approximately 1000–1500 ppm S (Mathez 1976; Ripley and Li 2013), approximately 0.3% sulfide melt is formed. This translates to an *R* of ~300, far lower than the modelled *R* values in global PGE deposits. To upgrade the sulfide melt droplets, equilibration with a large amount of sulfide undersaturated magma is required. Traditionally, it has been assumed this can be achieved by convection of the sulfide-bearing melt in large magma chambers (Naldrett et al., 2009), but recent geochronological data (Mungall et al. 2016; Scoates et al. 2021) questioned the existence of large magma chambers. Maier et al. (2022) have argued that sulfides in sills below the Platreef and Flatreef could have equilibrated during extensive lateral transport within the footwall sediments of the Bushveld Complex, but this model is difficult to envisage for the upper Flatreef.

To conclusively test the sulfide entrainment model, one needs to locate metal- and sulfide-enriched fine-grained sills or dykes of Bushveld parent magma composition in the floor of the northern lobe. All fine-grained marginal rocks that have been studied so far are relatively metal and sulfide poor (Barnes et al. 2010). It could be argued that it is unlikely that all magma influxes to the Bushveld Complex have been sampled. Also, the studied samples of fine-grained marginal rocks come mainly from the EBC. Nevertheless, the currently available evidence showing that the fine-grained sills have “normal” PGE contents and are sulfide undersaturated are hard to ignore. These data are consistent with a model whereby the Bushveld PGE were concentrated within, or very proximal to, the final magma chamber.

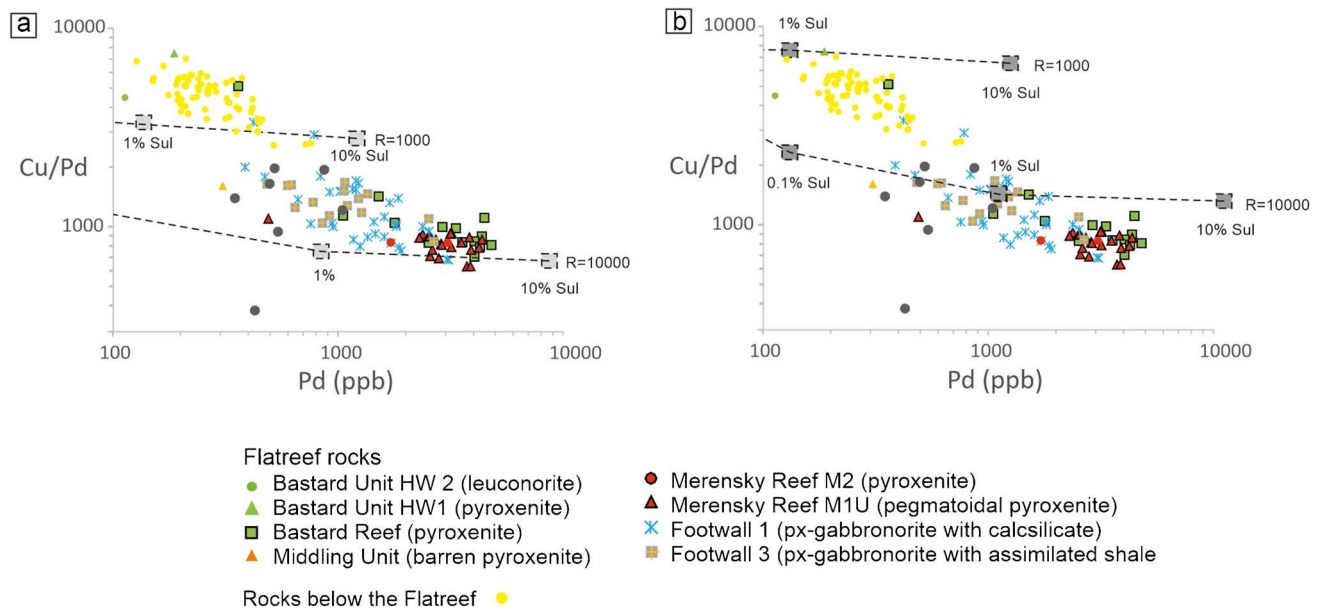


Fig. 13 Plot of Cu/Pd vs Pd for data from TMT006-D1, modelling R factors. **a** Model composition of sulfides assuming B1-B2 hybrid magma. **b** Assuming hybrid B1-B2 magma with added Cu (Maier et al. 2021a, b). Note that in (ii) model sulfide contents are broadly

in line with observed sulfide contents. In both models, we assumed D values between sulfide and silicate melt of 10^5 for Pd and 10^3 for Cu. Pd and Cu values for Bushveld B1 and B2 magmas are from Barnes et al. (2010)

Notably, neither the contamination nor the sulfide entrainment model provide an explanation for the trend of increasing sulfide mode with height in the upper Flatreef, observed in the TMT006 drill cores and across the entire Turfspruit property (Grobler et al. 2019). Maier et al. (2021b) have suggested that this trend reflects sulfide melt percolation through the Flatreef crystal mush. This model is evaluated in more detail below.

The role of sulfide melt percolation

In addition to its high budget of PGE and sulfide, the Flatreef is unusual in that elevated PGE, and sulfide contents are found essentially across its entire width, rather than in just a few narrow reefs as in the UCZ of the WBC and EBC (Grobler et al. 2019). It could be suggested that in the Flatreef, the sulfide melt percolated through a semi-solidified crystal pile (Hutchinson and McDonald 2008; Maier et al. 2021a, b) analogous to, but on a much larger scale than that found in the footwall of the Merensky Reef in the WBC (Leeb du Toit 1986; Barnes and Maier 2002; Naldrett et al. 2009; Smith et al., 2021). Maier et al. (2021b) suggested that sulfide percolation is consistent with the downward decreasing PGE contents in many of the drill cores on the Turfspruit property and the complimentary thickness variation of the mineralised BAR and the barren Middling: Where BAR is thick, the Middling is thin (Fig. 9), and vice versa, potentially because the Middling was locally transformed

into BAR by downward percolating sulfides with broadly similar metal tenors.

The textures of the mineralised rocks provide new constraints on the percolation model. Normally, sulfide droplets in orthocumulates tend not to wet the silicate minerals if there is silicate melt present. Instead, they form “stranded droplets” which are preserved as globular ores. However, if the grain size of the cumulates is large enough, the pore throats can be big enough for the smaller droplets to move through them in which case the sulfides can start to percolate. The more sulfides are present, the more they tend to join up, which increases the driving hydrostatic head to the point where it can overcome the capillary force and the droplets form interconnected migrating networks, displacing the intercumulus silicate melt upwards (Chung and Mungall 2009). This may give rise to domains of pure silicate-sulfide net textures a few grain sizes across, separated by domains of nearly sulfide-free orthocumulate (Fig. 7). Within the domains free of silicate melt, the sulfide liquid is able to wet the silicates. Thus, the process is self-reinforcing and can eventually result in net-textured ores (Barnes et al. 2017). In some cases, percolating sulfide opens up fractures in the cumulus network that get preserved as sulfide veins. These have traditionally been called “remobilisations”, but they may instead result from the strain-dependent rheology of the mush, which cracks like wet sand if it is strained fast enough (Barnes et al. 2020).

Intriguingly, the CT data (Fig. 8, ESM 1-S5, ESM 3) suggest that sulfides could percolate in only some of the

analysed samples. In the top sample (815.11–815.22 m), silicate grain size is ~ 5 mm requiring sulfide blebs of 15–30 mm to be able to percolate (Chung and Mungall 2009). However, virtually all sulfides are smaller than this threshold, assuming ~ 25% porosity (ESM1-S6). Some very small sulfides (< 1 mm) could have percolated, but the sample contains very few of those (< 5% of the total sulfides). In the basal sample (842.08–842.18 m), orthopyroxene grain size is larger (~ 1 cm), but none of the observed sulfides is above the 10 mm minimum size. In contrast, in the two pegmatoidal samples (823.58–823.68 m, 834.92–835.02 m), sulfides with sizes larger than about 10 mm make up 25–30% of the total population suggesting that in these samples the sulfides could have percolated.

Variability in the efficiency of sulfide melt percolation is also suggested by vertical and lateral differences in PGE trends on the Turfspruit property (Maier et al. 2021b). In the stratigraphically deeper portions of the Flatreef, Pt/Pd typically shows a broadly progressive decrease (ESM1-S7; Grobler et al. 2019) that is difficult to reconcile with sulfide melt percolation alone. In addition, pervasive sulfide melt percolation would be expected to result in bottom loading of PGE abundance in many drill cores. Such trends have been described previously above sedimentary rafts in the Platreef (Kinnaird et al. 2005) and at the base of the Platreef (Hutchinson and McDonald 2008), and additional examples from the Platreef on Turfspruit are shown in ESM1-S8 and ESM2-S4. However, most drill cores intersecting the deep Flatreef show a broad downward decrease in PGE contents, at increasing sulfide contents (Grobler et al. 2019). The vertical and lateral variability in PGE and sulfide content together with the variability in the size of the sulfides revealed by the CT data, and the petrographic evidence for early oikocryst formation in parts of the Merensky Reef (Smith et al., 2021) suggest that percolation is a local-scale phenomenon (Maier et al. 2021b). The process possibly resulted from fluidisation of the mush on 10 s of m scales triggered by channelised up-flow of melts and volatiles from the sedimentary floor rocks. One expression is the late-stage formation of anorthosite forming lenses, corona structures, and small diapirs (Maier et al., 2021a, b). Fluidisation allowed crystals to move past one another, increasing the effective radius of the pore throats. This may be a feedback-driven, self-organised process—a minor amount of fluidisation kicks the process off in some places but not others, but once percolation starts, it happens fast, due to runaway sulfide coalescence in the pores (Barnes et al. 2017). This can result in locally enhanced ore grades, both vertically and laterally, notably in the fluidisation channels and within layers of high porosity underlain by relatively impermeable adcumulates, sedimentary rafts or the floor of the intrusion.

Conclusions

The study of the Flatreef deposit since 2012 has generated a large amount of data that shed new light on the origin of the PGE mineralisation in the Bushveld northern lobe. Key results include the recognition of laterally extensive magmatic sills and sedimentary horizons in the lower Flatreef, the vastly higher amount of PGE and sulfides compared to the WBC reefs, the compositional and lithological evidence for contamination with the sedimentary host rocks of the Duitschland Formation, particularly in the lower portion of the Flatreef where this coincides with decreasing PGE grade, and the evidence for localised sulfide percolation within and below the main mineralised reefs and within the dolomites and hornfels floor rocks. The picture emerging is one of pronounced lateral and vertical compositional variability proposed to be caused by the following sequence of events:

- (i) The lower portions of the Flatreef formed when Bushveld magmas (possibly hybrids of B1-B2 magma types) injected into the Duitschland Formation and were substantially contaminated with sulfidic and Cu-rich pelitic-carbonaceous rocks during emplacement. The addition of significant external sulfur triggered sulfide melt immiscibility, explaining the high sulfide budget of the rocks (up to several per cent). The mass ratio of silicate to sulfide melt (*R* factor) was relatively low (as little as 1000), resulting in low PGE tenors (10–20 ppm in 100% sulfide).
- (ii) The upper portions of the Flatreef crystallised from magma influxes that were typically less contaminated, possibly due to lining of some of the magma conduits by the crystallisation products of earlier magma pulses. The magmas equilibrated at higher *R* factors resulting in elevated PGE tenors (200–300 ppm in 100% sulfide). Whether these high *R* factors were achieved during sulfide entrainment from depth or during magma emplacement into the Bushveld magma chamber remains unclear.
- (iii) The increased thickness of ultramafic cumulates relative to the Upper Critical Zone in the western and eastern Bushveld, notably in domains where the dip of the layering is relatively shallow, suggests that the cumulate mushes underwent granular flow, resulting in thickening of ultramafic cumulates in hydrodynamic traps.
- (iv) The sulfide and PGE contents of the rocks show strong lateral variation. High-grade intersections like the TMT006 drill cores may be adjacent to drill cores that show < 50% of the sulfur and metal budget.
- (v) In the upper portion of the TMT006 intersections and within sedimentary rafts of the lower Platreef, there is compositional and textural evidence for

localised downward percolation of sulfide melt, in the form of downward decreasing PGE grade and the interconnectivity and large grain size of the sulfides.

- (vi) In addition to downward migration of sulfide melt, there is evidence for upward migration of magma, in the form of small mushroom-shaped anorthosite diapirs within the Bastard Unit.

Supplementary information The online version contains supplementary material available at <https://doi.org/10.1007/s00126-022-01156-6>.

Acknowledgements We thank Albie Brits for discussions and Alexandra Crossingham for assistance in generating the figures and compiling data. Journal editor Georges Beaudoin, associate editor Marco Fiorentini and referees Dave Holwell and Katie McFall provided constructive reviews which are greatly appreciated.

Declarations

Conflict of interest No funding was received for conducting this study, but Ivanplats provided a large amount of whole rock data. The authors declare they have no financial interests. WDM is on the editorial board of *Mineralium Deposita*. He designed and leads the study. SJB conducted the micro XRF work. BMG conducted the X-ray CT work. WDS produced the FESEM element maps. All authors contributed to writing, review and editing.

Open Access This article is licensed under a Creative Commons Attribution 4.0 International License, which permits use, sharing, adaptation, distribution and reproduction in any medium or format, as long as you give appropriate credit to the original author(s) and the source, provide a link to the Creative Commons licence, and indicate if changes were made. The images or other third party material in this article are included in the article's Creative Commons licence, unless indicated otherwise in a credit line to the material. If material is not included in the article's Creative Commons licence and your intended use is not permitted by statutory regulation or exceeds the permitted use, you will need to obtain permission directly from the copyright holder. To view a copy of this licence, visit <http://creativecommons.org/licenses/by/4.0/>.

References

- Abernethy K (2020) Geochemistry and petrology of the Flatreef, as exposed in deep drill cores UMT 081 and 94, PhD thesis, Cardiff University, 309pp
- Ballhaus CG, Stumpff EF (1986) Sulfide and platinum mineralization in the Merensky Reef: evidence from hydrous silicates and fluid inclusions. *Contrib Mineral Petrol* 94:93–204
- Barnes SJ (2006) Komatiite-hosted nickel sulfide deposits: geology, geochemistry, and genesis. *Soc Econ Geol Spec Publ* 13:51–118
- Barnes S-J, Maier WD (2002) Platinum-group elements and microstructures of normal Merensky Reef from Impala Platinum mines, Bushveld Complex. *J Petrol* 43:103–128
- Barnes S-J, Maier WD, Curl E (2010) Composition of the marginal rocks and sills of the rustenburg layered suite, Bushveld Complex, South Africa: implications for the formation of the platinum-group element deposits. *Econ Geol* 105:1481–1511
- Barnes SJ, Mungall JE, Le Vaillant M, Godel B, Leshner CM, Holwell DA, Lightfoot PC, Krivolutskaya NA, Wei B (2017) Sulfide-silicate textures in magmatic Ni-Cu-PGE sulfide ore deposits: disseminated and net-textured ores. *Am Miner* 102:473–506
- Barnes SJ, Taranovic V, Miller JM, Boyce G, Beresford S (2020) Sulfide emplacement and migration in the Nova-Bollinger Ni-Cu-Co deposit, Albany-Fraser orogen, Western Australia. *Econ Geol* 115:1749–1776
- Barnes SJ, Latypov R, Chistyakova S, Godel B, Schoneveld LE (2021a) Idiomorphic oikocrysts of clinopyroxene produced by a peritectic reaction within a solidification front of the Bushveld Complex. *Contrib Miner Petrol* 176:1–19
- Barnes SJ, Ryan CG, Moorhead G, Latypov R, Maier WD, Yudovskaya M, Godel B, Schoneveld LE, Le Vaillant M, Pearce MB (2021b) Spatial association between platinum minerals and magmatic sulfides imaged with the Maia Mapper and implications for the origin of the chromite-sulfide-PGE association. *Canadian Mineralogist*, Online. <https://doi.org/10.3749/canmin.2000100>
- Barton JM, Cawthorn RG, White JA (1986) The role of contamination in the evolution of the Platreef of the Bushveld Complex. *Econ Geol* 81:1096–1108
- Beukes JJ, Roelofse F, Gauert CDK, Grobler DF, Ueckermann H (2021) Strontium isotope variations in the Flatreef and its immediate footwall and hanging wall on Macalakashop, Northern Limb, Bushveld Complex, Min Deposita 56:45–57
- Boudreau A (2019) Hydromagmatic processes and platinum-group element deposits in layered intrusions. Cambridge University Press, 275pp
- Buchanan DL, Nolan J, Suddaby P, Rouse JE, Viljoen MJ, Davenport JWJ (1981) The genesis of sulfide mineralization in a portion of the Potgietersrus limb of the Bushveld Complex. *Econ Geol* 76:568–579
- Cawthorn RG, Barton JR, Viljoen MJ (1985) Interaction of floor rocks with the Platreef on Overysel, Potgietersrus, northern Transvaal. *Econ Geol* 80:988–1006
- Davies G, Tredoux M (1985) The platinum-group element and gold contents of the marginal rocks and sills of the Bushveld Complex. *Econ Geol* 80:838–848
- Eales HV, Marsh JS, Mitchell AA, De Klerk WJ, Kruger FJ, Field M (1986) Some geochemical constraints upon models for the crystallization of the upper critical zone-main zone interval, northwestern Bushveld complex. *Mineralog Mag* 50:567–582
- Eales HV, Field M, de Klerk WJ, Scoon RN (1988) Regional trends of chemical variation and thermal erosion in the upper critical zone, western Bushveld Complex. *Mineralog Mag* 52:63–79
- Godel BM (2013) High-resolution x-ray computed tomography and its application to ore deposits: from data acquisition to quantitative three-dimensional measurements with case studies from Ni-Cu-PGE deposits. *Economic Geology* 108:2005–2019. <https://doi.org/10.2113/econgeo.108.8.2005>
- Godel BM, Barnes S-J, Maier WD (2006) 3-D distribution of sulphide minerals in the Merensky Reef (Bushveld Complex, South Africa) and the J-M reef (Stillwater Complex, USA) and their relationship to microstructures using X-ray computed tomography. *J Petrol* 47:1853–1872
- Godel BM, Barnes S-J, Maier WD (2007) The Merensky Reef of the Bushveld Complex, South Africa: a mass balance of platinum group elements in sulfide minerals, platinum group minerals and the whole rock. *J Petrol* 48:1569–1604
- Godel BM, Barnes SJ, Barnes S-J (2013) Deposition mechanisms of magmatic sulphide liquids: evidence from high-resolution x-ray computed tomography and trace element chemistry of komatiite-hosted disseminated sulphides. *J Petrol* 54:1455–1481. <https://doi.org/10.1093/petrology/egt018>
- Grobler DF, Brits JAN, Maier WD, Crossingham A (2019) Litho- and chemostratigraphy of the Flatreef PGE deposit, northern Bushveld Complex. *Miner Deposita*. <https://doi.org/10.1007/s00126-012-0436-1>

- Harris C, Chaumba JB (2001) Crustal contamination and fluid–rock interaction during the formation of the Platreef, northern limb of the Bushveld Complex, South Africa. *J Petrol* 42:1321–1347
- Holwell DA, Jordaan A (2006) Three-dimensional mapping of the Platreef at the Zwartfontein South mine: implications for the timing of magmatic events in the northern limb of the Bushveld Complex, South Africa. *Appl Earth Sci* 115:41–48
- Holwell DA, McDonald I (2007) Distribution of platinum-group elements in the Platreef at Overysel, northern Bushveld Complex: a combined PGM and LA-ICP-MS study. *Contrib Mineral Petrol* 154:171–190
- Holwell DA, Boyce AJ, McDonald I (2007) Sulfur isotope variations within the Platreef Ni-Cu-PGE deposit: genetic implications for the origin of sulfide mineralization. *Econ Geol* 102:1091–1110
- Hutchinson D, Kinnaird JA (2005) Complex multistage genesis for the Ni–Cu–PGE mineralisation in the southern region of the Platreef, Bushveld Complex, South Africa. *Appl Earth Sci* 114:208–224
- Hutchinson D, McDonald I (2008) Laser ablation ICP-MS study of platinum-group elements in sulphides from the Platreef at Turfspruit, northern limb of the Bushveld Complex, South Africa. *Miner Deposita* 43:695–711
- Ihlenfeld C, Keays RR (2011) Crustal contamination and PGE mineralization in the Platreef, Bushveld Complex, South Africa: evidence for multiple contamination events and transport of magmatic sulfides. *Miner Deposita* 46:813–832
- Keir-Sage E, Leybourne MI, Jugo PJ, Grobler DF, Mayer CC (2021) Assessing the extent of local crust assimilation within the Flatreef, northern limb of the Bushveld Igneous Complex, using sulfur isotopes and trace element geochemistry. *Miner Deposita* 56:91–102
- Kekana SM (2014) An investigation of mineralisation controls in the upper section of the Platreef in the southern sector, on Turfspruit, Northern Limb, Bushveld Complex, South Africa. MSc thesis, Univ Witwatersrand, SA, 128pp
- Kennedy B (2018) Unconventional olivine-rich cumulates, magma dynamics and development of platinum-group element mineralisation in the Main Zone of the northern Bushveld Complex (Doctoral dissertation, Cardiff University).
- Kinnaird JA, Hutchinson D, Schurmann L, Nex PAM, de Lange R (2005) Petrology and mineralization of the southern Platreef: northern limb of the Bushveld Complex, South Africa. *Min Deposita* 40:576–597
- De Klerk WJ (1982) The geology, geochemistry and silicate mineralogy of the upper critical zone of the north-western Bushveld complex, at Rustenburg Platinum Mines, Union Section. Rhodes University, MSc thesis (unpublished), 210pp
- De Klerk WJ (1992) Petrogenesis of the upper critical zone of the Western Bushveld Complex with emphasis on the UG1 footwall and Bastard Units. Ph.D thesis, Rhodes University, Grahamstown: 294pp
- Leeb-du Toit A (1986) The Impala Platinum mines. In: Anhaeusser CR, Maske S (eds) *Mineral deposits of Southern Africa*. Geol Soc S Afr, Johannesburg, 1091–1106.
- Leshner CM, Burnham OM (2001) Multicomponent elemental and isotopic mixing in Ni–Cu–(PGE) ores at Kambalda, Western Australia. *Can Mineral* 39:421–446
- Li C, Ripley EM, Merino E, Maier WD (2004) Replacement of base metal sulfides by actinolite, epidote, calcite, and magnetite in the UG2 and Merensky Reef of the Bushveld Complex, South Africa. *Econ Geol* 99:173–184
- Maier WD (2005) Platinum-group element (PGE) deposits and occurrences: mineralization styles, genetic concepts, and exploration criteria. *J Afr Earth Sc* 41:165–191
- Maier WD, Barnes S-J (2008) Platinum-group elements in the UG1 and UG2 chromitites and the Bastard reef at Impala platinum mine, western Bushveld Complex. *S Afr J Geol* 111:159–176
- Maier WD, Barnes S-J (2010) The petrogenesis of PGE reefs in the upper main zone of the northern lobe of the Bushveld Complex on the farm Moorddrift, South Africa. *Econ Geol* 105:841–854
- Maier WD, Barnes S-J, Groves DI (2013) The Bushveld Complex, South Africa: formation of platinum-palladium, chrome and vanadium-rich layers via hydrodynamic sorting of a mobilized cumulate slurry in a large, relatively slowly cooling, subsiding magma chamber. *Mineral Deposita* 48:1–56
- Maier WD, Barnes S-J, Karykowski BT (2016) A chilled margin of komatiite and Mg-rich basaltic andesite in the western Bushveld Complex. South Africa *Contrib Mineral Petrol*. <https://doi.org/10.1007/s00410-016-1257-5>
- Maier WD, Abernethy KEL, Grobler DF, Moorhead G (2021a) Formation of the Flatreef deposit, northern Bushveld, by hydrodynamic and hydromagmatic processes. *Miner Deposita* 56:11–30
- Maier WD, Barnes S-J, Muir D, Savard D, Lahaye Y, Smith WD (2021b) Formation of Bushveld anorthosite by reactive porous flow. *Contrib Miner Petrol* 176:1–12
- Maier WD, Brits A, Grobler D (2022) Petrogenesis of PGE mineralised intrusions in the floor of the northern Bushveld Complex. *South African J Geol*. <https://doi.org/10.25131/sajg.125.0019>
- Maier WD, De Klerk L, Blaine J, Manyeruke T, Barnes S-J, Stevens MVA, Mavrogenes JA (2008) Petrogenesis of contact-style PGE mineralization in the northern lobe of the Bushveld Complex: comparison of data from the farms Rooipoort, Townlands, Drenthe and Nonnenwerth. *Mineralium Deposita* 43:255–280
- Maier WD, Eales HV (1997) Correlation within the UG2-Merensky Reef interval of the Western Bushveld Complex, based on geochemical, mineralogical and petrological data. *Bulletin 20*. Council for Geoscience: 56pp
- Manyeruke T, Maier WD, Barnes S-J (2005) Major and trace element geochemistry of the Platreef on the farm Townlands, northern Bushveld Complex. *S Afr J Geol* 108:379–394
- Mathez EA (1976) Sulfur solubility and magmatic sulfides in submarine basalt glass. *J Geophys Res* 81:4269–4276
- Mathez EA, Kinzler RJ (2017) Metasomatic chromitite seams in the Bushveld and Rum intrusions. *Elements* 13:397–402
- McBirney AR, Noyes RM (1979) Crystallization and layering in the Skaergaard intrusion. *J Petrol* 20:487–554
- McDonald I, Holwell DA (2007) Did lower zone magma conduits store PGE-rich sulphides that were later supplied to the Platreef? *S Afr J Geol* 110:611–616
- Meurer WP, Klaber SA, Boudreau AE (1997) Discordant bodies from olivine-bearing zones III and IV of the Stillwater complex, Montana—evidence for post-cumulus fluid migration in layered intrusions. *Contrib Mineral Petrol* 130:81–92
- Mitchell AA, Manthorpe R (2002) The Giant Mottled Anorthosite: a transitional sequence at the top of the upper critical zone of the Bushveld Complex. *S Afr J Geol* 105:15–24
- Mitchell AA, Scoon RN (2012) The Platreef of the Bushveld Complex, South Africa: a new hypothesis of multiple, non-sequential magma replenishment based on observations at the Akanani Project, north-west of Mokopane. *S Afr J Geol* 115:535–550
- Mungall JE, Kamo S, McQuade S (2016) U-Pb geochronology documents out-of-sequence emplacement of ultramafic layers in the Bushveld Igneous Complex of South Africa. *Nat Commun* 7:1–13
- Naldrett AJ, Wilson A, Kinnaird J, Chunnett G (2009) PGE tenor and metal ratios within and below the Merensky Reef, Bushveld Complex: implications for its genesis. *J Petrology* 50:625–659
- Prichard HM, Barnes S-J, Maier WD, Fisher PC (2004) Variations in the nature of the platinum-group minerals in a cross-section through the Merensky Reef at Impala Platinum: implications for the mode of formation of the reef. *Can Mineral* 42:423–437
- Ripley EM, Li C (2013) Sulfide saturation in mafic magmas: is external sulfur required for magmatic Ni-Cu-(PGE) ore genesis? *Econ Geol* 108:45–58

- Scoates JS, Wall CJ, Friedman RM, Weis D, Mathez EA, VanTongeren JA (2021) Dating the Bushveld Complex: timing of crystallization, duration of magmatism, and cooling of the world's largest layered intrusion and related rocks. *Journal of Petrology* 62:egaa107
- Scoon RN, Costin G, Mitchell AA, Moine B (2020) Non-sequential injection of PGE-rich ultramafic sills in the Platreef Unit at Aka-nani, Northern Limb of the Bushveld Complex: evidence from Sr and Nd isotopic systematics. *Journal of Petrology* 61:egaa032
- Sharman ER, Penniston-Dorland SC, Kinnaird JA, Nex PAM, Brown M, Wing BA (2013) Primary origin of marginal Ni-Cu-(PGE) mineralization in layered intrusions: $\Delta^{33}\text{S}$ evidence from The Platreef, Bushveld, South Africa. *Econ Geol* 108:365–377
- Smith WD, Maier WD, Barnes SJ, Moorhead G, Reid D, Karykowski B (2021) Element mapping the Merensky Reef of the Bushveld Complex. *Geosci Front* 12:101101
- Stephenson H (2018) The Platreef magma event at the world-class Turfspruit Ni-Cu-PGE deposit: implications for mineralisation processes and the Bushveld Complex stratigraphy (Doctoral dissertation, Cardiff University).
- Viljoen MJ, de Klerk WJ, Coetzer PM, Hatch NP, Kinloch E, Peyerl W (1986) The Union section of Rustenburg Platinum Mines Ltd with reference to the Merensky Reef. In: Anhaeusser CR, Maske S (eds) Mineral deposits of Southern Africa. Geol Soc S Afr, Johannesburg 1061–1090.
- Wallmach T, Hatton CJ, Droop GTR (1989) Extreme facies of contact metamorphism developed in calc silicate xenoliths in the eastern Bushveld Complex. *Can Min* 27:509–523
- Yudovskaya M, Belousova E, Kinnaird J, Dubinina E, Grobler DF, Pearson N (2017) Re-Os and S isotope evidence for the origin of Platreef mineralization (Bushveld Complex). *Geochim Cosmochim Acta* 214:282–307
- Yudovskaya MA, Sluzhenikin SF, Costin G, Shatagin KN, Dubinina EO, Grobler DF, Ueckermann H, Kinnaird JA (2018) Anhydrite assimilation by ultramafic melts of the Bushveld Complex, and its consequences to petrology and mineralization. *SEG Special Publications* 21:177–206
- Yudovskaya MA, Costin G, Sluzhenikin SF, Kinnaird JA, Ueckermann H, Abramova VD, Grobler DF (2021) Hybrid norite and the fate of argillaceous to anhydritic shales assimilated by Bushveld melts. *Miner Deposita* 56:73–90
- Zhitova LM, Kinnaird JA, Gora MP, Shevkoa EP (2016) Magmatogene fluids of metal-bearing reefs in the Bushveld Complex, South Africa: based on research data on fluid inclusions in quartz. *Geol Ore Deposits* 58:58–81

Publisher's note Springer Nature remains neutral with regard to jurisdictional claims in published maps and institutional affiliations.